

1 **Drivers of the  $\delta^{18}\text{O}$  Changes in Indian Summer Monsoon Precipitation between**  
2 **the Last Glacial Maximum and Pre-industrial Period**

3

4 Thejna Tharammal <sup>1\*</sup>, Govindasamy Bala<sup>2</sup>, Jesse Nusbaumer<sup>3</sup>

5

6 <sup>1</sup> Interdisciplinary Centre for Water Research, Indian Institute of Science, Bengaluru  
7 560012, India

8 <sup>2</sup> Centre for Atmospheric and Oceanic Sciences, Indian Institute of Science,  
9 Bengaluru 560012, India

10 <sup>3</sup> National Center for Atmospheric Research, Boulder, USA

11 Corresponding author: [thejnat@iisc.ac.in](mailto:thejnat@iisc.ac.in)

12

13

14

15

16

17

18

19

20

21

22

23

24

25

26

27

28

29

30

31

32 **Abstract**

33 In this study, we investigate the changes in water isotope ratios in the Indian summer  
34 monsoon precipitation ( $\delta^{18}\text{O}_{\text{precip}}$ ) during the Last Glacial Maximum (LGM, ~21 ka  
35 Before Present) compared to the pre-industrial (PI) period, and the mechanisms  
36 driving these changes, using a general circulation model with water isotope and  
37 novel water vapor source-tagging capabilities.

38 During the LGM, the model simulates a substantial reduction (15%) in monsoon  
39 precipitation over the Indian subcontinent, consistent with proxy records. This drying  
40 in LGM is associated with reduced atmospheric water vapor, a thermodynamic  
41 response to cooling, while the westerly circulation, a dynamics response, is  
42 strengthened over parts of the subcontinent. Additionally, zonal temperature  
43 gradients between a relatively less-cooled tropical Western Pacific Ocean and Indian  
44 subcontinent lead to anomalous subsidence over the Indian region, enhancing the  
45 drying. Water vapor source tagging shows that while the four dominant moisture  
46 sources for the monsoon (South Indian Ocean, Arabian Sea, Indian land recycling,  
47 and Central Indian Ocean) remained the same, their contributions were reduced  
48 during the LGM. The  $\delta^{18}\text{O}_{\text{precip}}$  values over the Indian monsoon region are enriched  
49 by approximately 1‰ in the LGM simulation, and we find that this enrichment was  
50 not driven by the local amount effect. A decomposition analysis shows that the  
51 enrichment was primarily caused by reduced contributions from distant, isotopically  
52 depleted water vapor sources and secondarily by reduced rainout during moisture  
53 transport from the Indian Ocean.

54 These findings have important implications for paleoclimate reconstructions,  
55 suggesting that  $\delta^{18}\text{O}$  records from the Indian region could be indicators of broad-  
56 scale atmospheric circulation rather than being direct proxies for local precipitation  
57 amount.

58

59

60

61

62 **1. Introduction**

63 The Indian summer monsoon (ISM) system, occurring during the months of June-  
64 September, is one of the major climate features in the world. It sustains the  
65 livelihoods of more than a billion people in the subcontinent by contributing almost  
66 80% of the annual precipitation in the region. Monsoons were historically viewed as  
67 regional sea breezes driven by differential heating of land and sea. However, they  
68 are now understood as interconnected components of a global monsoon system,  
69 driven by the migration of Intertropical Convergence Zone (ITCZ), influencing tropical  
70 and subtropical precipitation (Gadgil 2003; Geen et al. 2020).

71  
72 Recent decades have seen increasing ISM intensification, characterized by more  
73 frequent extreme rainfall events and increased variability, likely due to anthropogenic  
74 climate change (Krishnan et al. 2016, 2020; Wang et al. 2020; Chen et al. 2020;  
75 Katzenberger et al. 2021; Kong et al. 2022; Mukherjee et al. 2024). However, there  
76 is considerable uncertainty in these future projections (Krishnan et al. 2020). Even  
77 small changes in the monsoon patterns can adversely affect the annual rainfall  
78 (~10% reduction in the ISM precipitation from the mean is classified as drought;  
79 Shewale and Kumar 2005), hence, it is important to understand the changes and  
80 variability in the monsoon rainfall. Paleoclimate studies using climate archives and  
81 proxy records provide crucial constraints for reducing uncertainties in future climate  
82 projections (Tierney et al. 2020a; Lohmann et al. 2020; Rehfeld et al. 2020; Brovkin  
83 et al. 2021; Kageyama et al. 2024). They are useful to understand the sensitivity of  
84 the monsoon systems to climate factors such as changes in greenhouse gases  
85 (GHG), orbital parameters, continental ice sheets, and Sea Surface Temperature  
86 (SST).

87  
88 The Last Glacial Maximum-LGM, about 23000 to 19000 years before present, is a  
89 period of high interest in climate change studies. LGM presents a valuable case  
90 study for understanding how the Earth's climate system responded to reduced CO<sub>2</sub>,  
91 presence of the Laurentide ice sheets and ice-sheet topography, and orbital forcing.  
92 The abundance of proxy-climate records for this period facilitates comparisons  
93 between proxy data and models. Climate records from the Indian Summer Monsoon  
94 region such as, water isotope records from sedimentary cores and speleothems

Deleted: the influence of

96 (Contreras-Rosales et al. 2014; Sinha et al. 2015; Kathayat et al. 2016; Liu et al.  
97 2021) indicate that LGM was characterised by a weaker Indian Summer Monsoon.  
98 Climate modeling studies suggest that the general reduction in precipitation over the  
99 globe during the LGM is mainly due to the cooling driven by lower greenhouse gas  
100 concentrations and the expansion of ice sheets (Broccoli and Manabe 1987, 2008;  
101 Yanase and Abe-Ouchi 2007; Tharammal et al. 2013; Kageyama et al. 2020; McGee  
102 2020; Seltzer et al. 2024). Further, the associated cooler sea surface temperatures  
103 in the tropics during the LGM (MARGO Project Members 2009; DiNezio et al. 2018;  
104 Tierney et al. 2020b) likely influenced the strength of the monsoon circulation,  
105 weakening the precipitation.

106  
107 Stable isotopes of water undergo temperature-dependent fractionation during phase  
108 changes. The resulting variations in the ratios of heavy to light isotopes ( $\delta$ -values)  
109 serve as powerful tracers of hydrological and atmospheric processes (Galewsky et  
110 al. 2016; Dee et al. 2023; Bailey et al. 2024). Records of water isotopes in the  
111 climate archives such as speleothems, tree rings, and sediment records are one of  
112 the major proxies in reconstructing the Indian monsoon precipitation (Yadava et al.  
113 2004; Maher 2008; Contreras-Rosales et al. 2014; Sinha et al. 2015; Kathayat et al.  
114 2016). To interpret these climate records, *the amount effect* (Dansgaard 1964),  
115 which is the observed inverse relationship between the ratio of water isotopes in  
116 precipitation ( $\delta^{18}\text{O}_{\text{precip}}$ ) and the amount of precipitation in the tropical regions, is  
117 used. The amount effect is related to depletion of water vapor of heavier isotopes  
118 during intense precipitation events, especially in convectively active tropical  
119 monsoon regions (Risi et al. 2008; Lee et al. 2008; Tharammal et al. 2017).  
120 However, the local precipitation amount is not the only factor that determines the  
121 isotopic composition of precipitation in the tropics. It is also influenced by other  
122 factors such as, relative contributions of moisture from various water vapor sources,  
123 atmospheric circulation, and upstream convection (Lewis et al. 2010; Breitenbach et  
124 al. 2010; Pausata et al. 2011; Sjolte and Hoffmann 2014; Zhu et al. 2017; Tabor et  
125 al. 2018; Konecky et al. 2019; Hu et al. 2019; Tharammal et al. 2023; Chakraborty et  
126 al. 2025). This complexity leads to considerable uncertainty in interpreting  $\delta^{18}\text{O}$   
127 records from the ISM region. Further, uncertainties remain in inferring the water  
128 isotope proxy records due to low data resolution and sparse coverage.

129

130 While proxy records have been used to study past changes in the Indian monsoon  
131 (Yadava et al. 2004; Dutt et al. 2015; Sinha et al. 2015; Kathayat et al. 2016;  
132 Kaushal et al. 2018), climate model studies focussed on the Indian monsoon  
133 precipitation and water isotope ratios during the LGM are largely lacking. Recent  
134 advancements in climate models equipped with water isotope tracers in their  
135 hydrology, along with the capabilities of tracking the evaporative water (Brady et al.  
136 2019) will enable us to find the climatic factors affecting the  $\delta^{18}\text{O}_{\text{precip}}$  of monsoon  
137 precipitation, and also differentiate the moisture sources and their effects on the  
138  $\delta^{18}\text{O}_{\text{precip}}$  (Hu et al. 2019; Kathayat et al. 2021; He et al. 2021; Tharammal et al.  
139 2023). Therefore, applying these novel modeling techniques to resolve the drivers of  
140  $\delta^{18}\text{O}_{\text{precip}}$  change in the Indian region during the LGM is a key research gap that this  
141 study aims to fill.

142

143 In this study, we examine the mechanisms behind the changes in the monsoon  
144 precipitation and water isotope ratios in the ISM region during the LGM using a  
145 climate model with water isotope and novel water vapor source-tagging capabilities.  
146 We will analyse the responses of water isotopes in precipitation, and moisture  
147 sources to the glacial climate, and importantly, identify the major physical processes  
148 influencing the changes in the isotopic ratios of precipitation. We will analyse the  
149 relative importance of the "amount effect" compared to changes in moisture source  
150 and transport in influencing the  $\delta^{18}\text{O}_{\text{precip}}$  values during the LGM.

151

152 The paper is structured as follows: In Section 2, we introduce the model simulations  
153 and methods. Section 3 includes the assessment of model performance under the PI  
154 climate, analysis of changes in the monsoon, water vapor sources, and isotope  
155 ratios of precipitation in the LGM simulation. Section 4 includes a discussion of the  
156 results and main conclusions of the study.

157

## 158 **2. Methods**

### 159 **2.1 Climate Model**

160 Our study uses the Community Earth System Model, CESM version 1.2 with water  
161 isotope tracking capabilities (iCESM, Brady et al. 2019) from the National Center for

162 Atmospheric Research (NCAR) for the climate simulations. Atmospheric and land  
163 components of the iCESM are isotopic versions of the Community Atmosphere  
164 Model CAM version 5.3 and Community Land Model CLM version 4, respectively.  
165 The sea-ice model in the iCESM is Los Alamos Sea Ice Model version 4 (CICE4),  
166 which is run in prescribed sea ice mode for the simulations presented here. The  
167 isotope tracking in the model is facilitated with the inclusion of a parallel hydrologic  
168 cycle for the water isotope tracers in the iCESM. It follows the water isotope ratios,  
169 fluxes, and isotopic fractionations on phase changes in the components of the  
170 hydrologic cycle (Brady et al. 2019).  
171 iCESM has proven successful in reproducing the present global distribution of  
172 isotopes in precipitation (Brady et al. 2019). Further, the model includes a tagging  
173 feature for the evaporated water and can be used to track the sources of water vapor  
174 for precipitation in a sink region. The model was successfully used in several studies  
175 to reconstruct the past and present climate and isotope ratios in precipitation, and to  
176 track the sources of water vapor in various tropical regions (Tabor et al. 2018; Hu et  
177 al. 2019; Windler et al. 2020; He et al. 2021; Tharammal et al. 2023).  
178

## 179 **2.2 Experiments**

180 We conducted two time-slice simulations for the current study, a) the pre-industrial  
181 (PI) control experiment and b) the LGM simulation, with prescribed SSTs, sea ice  
182 extent, and prescribed ocean surface isotopic ratios.

183 The isotopic composition of meteoric water is represented by the delta ( $\delta$ ) value in  
184 permil (‰) units in the paper, denoting the relative abundance of the ratio of heavy  
185 isotope to the light isotope in a sample with respect to a geochemical standard  
186 (VSMOW-Vienna Standard Mean Ocean Water).

187 Accordingly,  $\delta^{18}\text{O}$  is  $(R_{\text{sample}}/R_{\text{VSMOW}} - 1) \times 1000$ . R is the ratio of heavy to the light  
188 isotope,  $^{18}\text{O}/^{16}\text{O}$ .  $R_{\text{VSMOW}}$  is the standard isotope ratio.

189

190 For the PI simulation, the orbital conditions, GHG, SST, sea ice extent, and aerosol  
191 boundary conditions are set at the year 1850. The GHG and orbital boundary  
192 conditions of the experiments are given in Table S1. The SST and sea ice fraction  
193 data for the PI experiment are derived from the corresponding coupled CESM

194 simulation (Zhu and Poulsen 2021). A uniform sea-surface  $\delta^{18}\text{O}$  of 0.5‰ is  
195 prescribed for the control simulation. This is an approximate value based on present-  
196 day observations and is close to the observed surface values of the tropical and  
197 subtropical oceans (Hoffmann and Heimann 1997; LeGrande and Schmidt 2006; Lee  
198 and Fung 2008).

199 For the LGM simulation, we follow the Paleoclimate Modelling Intercomparison  
200 Protocol version 4 (PMIP4; Kageyama et al. 2020), and the GHG, orbital parameters,  
201 land-sea mask, and surface topography are set to 21 ka BP conditions. The ice  
202 sheet extent and topography for the LGM experiment (Fig. S1a) are derived from the  
203 ICE-6G ice sheet reconstructions by Peltier et al. (2015). The coastlines for the LGM  
204 experiment are adapted from the ICE-6G reconstruction and represent a lowering of  
205 sea level by 120m during the LGM (Lambeck et al. 2014). The SST and sea ice  
206 fraction for the LGM simulation (Fig. S1b, c) are obtained from the CESM coupled  
207 LGM simulation (Zhu and Poulsen 2021). The formation of large continental ice  
208 sheets during the LGM led to enrichment of heavier isotopes in the seawater oxygen  
209 isotope ratios (ice-volume effect, Lambeck 2000). It is widely accepted that the sea  
210 surface water isotope ratios during the LGM were approximately 1‰ enriched  
211 compared to the pre-industrial values (Duplessy et al. 2002; [Sima et al. 2006](#)). We  
212 represent this in the LGM simulation by prescribing a uniform sea surface  
213 enrichment of water isotopes by 1‰ for  $\delta^{18}\text{O}$ , compared to the PI value.

214 Further, to identify the effects of water vapor sources on the monsoon precipitation  
215 and water isotopes during the LGM, we tag the evaporated vapor from 17 ocean and  
216 land regions in and around the ISM region in both the PI and the LGM experiments  
217 (tagged regions are shown in Fig. S2a). The simulations are run for 30 years, and  
218 the last 20 years are used for the analysis.

219

## 220 **2.3 Monsoon circulation indices and moisture budget analysis**

### 221 **2.3.1 Monsoon circulation indices**

222 Strength of the monsoon circulation can be estimated using various indices (Li et al.  
223 2024). We calculate the monsoon circulation strength in PI and LGM simulations  
224 using the following six indices selected to capture both circulation changes and water  
225 vapor transport related to the monsoon precipitation. The geographical domains  
226 used for the estimation of these indices are shown in Figure S2b.

Deleted: Sima et al. 2006;

228 1) The Somali jet index (Boos and Emanuel 2009), which is calculated as the square  
229 root of twice the domain mean kinetic energy ( $\sqrt{2\overline{KE}}$ ) of the 850 hPa horizontal  
230 wind over the region, [5°S - 20°N, 50°E - 70°E].

231  
232 2) The hydrological index, following (Fasullo and Webster 2003), calculated by  
233 averaging the Vertically Integrated Moisture Transport (VIMT) in the Indian Ocean-  
234 Arabian Sea region, [20°S-30°N, 40°E-100°E]. VIMT is the total horizontal movement  
235 of water vapor in a vertical column of the atmosphere, and we calculate the term  
236 from the surface up to 300 hPa.

237 
$$\text{VIMT} = \frac{1}{g} \int_{P_{\text{surface}}}^{P_{\text{top}}} q \mathbf{V} dp \quad \text{----- (1)}$$

238  
239 Magnitude of VIMT is,

240 
$$|\vec{\text{VIMT}}| = \sqrt{\text{VIMT}_u^2 + \text{VIMT}_v^2} \quad \text{----- (2)}$$

241 Where P is atmospheric pressure, g is gravity, q is the specific humidity, and V is the  
242 wind vector with zonal and meridional components u and v.

243 3) Mid-tropospheric temperature gradient ( $\Delta T$ ), defined as the tropospheric  
244 temperature difference between a northern region and a southern region in the larger  
245 monsoon domain (Xavier et al. 2007).  $\Delta T$  signifies the cross-equatorial temperature  
246 gradient, and the onset of the ISM is defined as the time when  $\Delta T$  changes from  
247 negative to positive.

248 4) The vertical shear of zonal winds, following (Webster and Yang 1992), calculated  
249 as the difference between 200 hPa and 850 hPa zonal winds (U200-U850),  
250 averaged over the region 10°N-30°N, 50°E-95°E.

251 5) The meridional shear of the 850 hPa zonal wind (barotropic shear,  $-\partial u/\partial y$ ) over the  
252 region 10°N-26°N, 70°E-90°E that indicates magnitude of the cyclonic shear of the  
253 low-level monsoon circulation.

254 6) Various studies (Xue et al. 2003; Kripalani et al. 2007; [Vidya et al. 2020](#); Azhar et  
255 al. 2023) highlight a strong dependence of ISM circulation strength on the sea level  
256 pressure difference between the Mascarene High in the Southern Indian Ocean (MH;  
257 20°S-40°S, 45°E-100°E) and the wider ISM region (10°N-35°N, 45°E-100°E).

258 Therefore, this sea level pressure difference is also treated as an ISM index for this  
259 study.

Deleted: 
$$\text{VIMT} = \frac{1}{g} \int_{P_{\text{surface}}}^{P_{\text{top}}} qV dp$$

Deleted: P J

262 **2.3.2 Moisture budget calculations**

263 To understand the mechanisms driving the changes in monsoon precipitation, we  
 264 conducted a moisture budget analysis based on the framework of Chou and Lan  
 265 (2012). In this analysis, the net precipitation over a region (Precipitation-Evaporation,  
 266 P-E) is balanced by the vertically integrated moisture flux convergence in steady  
 267 state conditions.

268  
 269 This convergence term is then decomposed into contributions from vertically  
 270 integrated horizontal advection- the transport of water vapor,  $q$ , by horizontal winds,  
 271  $-(u \partial q / \partial x + v \partial q / \partial y)$ , and **vertical advection**- the transport of moisture by vertical  
 272 atmospheric motion,  $(-\omega \partial q / \partial p)$ , such that:

273 
$$P - E = - \left\langle u \left( \frac{\partial q}{\partial x} \right) + v \left( \frac{\partial q}{\partial y} \right) \right\rangle - \left\langle \omega \left( \frac{\partial q}{\partial p} \right) \right\rangle$$
  
 274 
$$\text{----- (3)}$$

275  
 276 The **angle brackets** denote pressure, mass-weighted vertical integration.  $u$ ,  $v$ , and  $\omega$   
 277 are the zonal, meridional, and vertical wind components.

278 A further decomposition of the advection terms into thermodynamic and dynamic  
 279 components to differentiate the contributions from the changes in water vapor and  
 280 circulation (e.g., Chou et al. 2009; Chou and Lan 2012) was not performed, as it is  
 281 beyond the scope of this study.

282 **2.4 Decomposition of  $\delta^{18}O_{precip}$  changes**

283 To diagnose the mechanisms driving the changes in precipitation-weighted  $\delta^{18}O_{precip}$   
 284 in the ISM region between the LGM and PI simulations, we perform a decomposition  
 285 analysis following the framework of Tabor et al. (2018). Using our water vapor  
 286 tagging results, this method expresses the total change in precipitation-weighted  
 287  $\delta^{18}O_{precip}$  ( $\delta^{18}O_p$  in the equations below) in the ISM domain as the sum of  
 288 contributions from each of the 17 tagged source regions.

289 
$$\Delta \delta^{18}O_p = \sum_{i=1}^{i=17} \left[ \left( \delta^{18}O_{p_i} \times \frac{p_i}{p_{total}} \right)_{LGM} - \left( \delta^{18}O_{p_i} \times \frac{p_i}{p_{total}} \right)_{PI} \right] \text{----- (4)}$$
  
 290

Deleted: (  
 Deleted: ,  
 Deleted: ,  
 Deleted: -[u(∂q/∂x)+v(∂q/∂y)]  
 Deleted: ,  
 Deleted: vertical advection  
 Deleted: -[ω(∂q/∂p)]  
 Deleted: .  
 Deleted: P-E=- <u(∂q/∂x)+v(∂q/∂y)> - <ω(∂q/∂p)>,  
 Deleted: s <>

301 where  $\delta^{18}O_{pi}$  is the isotopic ratio of precipitation at the ISM domain of water vapor  
 302 source i, and  $(p_i/p_{total})$  is the relative contribution of precipitation from source i to the  
 303 total precipitation at the ISM domain.

304 Further, the decomposition method isolates two primary effects on the change in  
 305 each  $\delta^{18}O_{pi}$  between LGM and PI: 1) contributions from changes in the isotopic  
 306 composition of each source tag between LGM and PI (First term on the right in Eqn.  
 307 5), and 2) the effect of changes in the relative precipitation contribution from the  
 308 water vapor sources (Second term on the right in Eqn. 5).

$$\Delta(\delta^{18}O_p)_i = \underbrace{(\delta^{18}O_{p_i,LGM} - \delta^{18}O_{p_i,PI}) \times \left(\frac{p_i}{p_{total}}\right)_{PI}}_{\text{Change in Isotopic Value}} + \delta^{18}O_{p_i,PI} \times \underbrace{\left(\left(\frac{p_i}{p_{total}}\right)_{LGM} - \left(\frac{p_i}{p_{total}}\right)_{PI}\right)}_{\text{Change in Relative Precipitation Contribution}}$$

309  
 310 --(5)

311 For each tag, the first term on the right can further be decomposed to three isotopic  
 312 effects: (i) the source effect, due to changes in  $\delta^{18}O$  of water vapor at the source  
 313 region, (ii) rainout effect, the changes in  $\delta^{18}O_{pi}$  of source tags due to changes in  
 314 rainouts on the path, and (iii) condensation effect, the enrichment of  $\delta^{18}O_{pi}$  at the sink  
 315 during condensation from the ambient vapor. The three terms are calculated as:

$$\Delta\delta^{18}O_{source,i} = (\delta^{18}O_{wv_{source},LGM} - \delta^{18}O_{wv_{source},PI}) \times \left(\frac{p_i}{p_{total}}\right)_{PI} \quad \text{--- (6)}$$

316  
 317

$$\Delta\delta^{18}O_{rainout,i} = [(\delta^{18}O_{wv_{sink}} - \delta^{18}O_{wv_{source}})_{LGM} - (\delta^{18}O_{wv_{sink}} - \delta^{18}O_{wv_{source}})_{PI}] \times \left(\frac{p_i}{p_{total}}\right)_{PI}$$

318  
 319 - (7)

$$\Delta\delta^{18}O_{condensation,i} = [(\delta^{18}O_{p_{sink}} - \delta^{18}O_{wv_{sink}})_{LGM} - (\delta^{18}O_{p_{sink}} - \delta^{18}O_{wv_{sink}})_{PI}] \times \left(\frac{p_i}{p_{total}}\right)_{PI}$$

320  
 321 -- (8)

322  $\delta^{18}O_{wv_{source}}$  and  $\delta^{18}O_{wv_{sink}}$  are the isotope ratios of water vapor at 850 hPa  
 323 (representing low level vapor, also level of monsoon low-level jet) of each tag at their  
 324 source and at the Indian sink, respectively.

325 Hence, we can quantitatively assess the driving mechanisms responsible for the  
 326 difference in total precipitation  $\delta^{18}O_{precip}$  between the LGM and PI climates.

327 **3. Results**

328 **3.1 PI control simulation**

329 **3.1.1 Monsoon in the PI control climate**

330 The model successfully simulates both the annual cycle and the summer monsoon  
331 (mean of June-July-August-September, JJAS) precipitation, also the south westerly  
332 winds over the ISM domain (8°N-30°N and 65°E-88°E; Fig. 1). The summer  
333 monsoon precipitation accounts for approximately 80% of the total annual  
334 precipitation, in agreement with the GPCP observational data (Adler et al. 2018).  
335 However, the iCESM overestimates the summer monsoon precipitation by ~20%  
336 (Fig. 1c). This wet bias has been reported in previous studies that used the CESM  
337 model (e.g. Pathak et al. 2019; Hanf and Annamalai 2020) and they attribute this  
338 bias to factors such as, model resolution, biases in simulated circulation, and  
339 convective parameterizations.  
340

341 **3.1.2 Water isotopes in the PI monsoon precipitation**

342 The domain mean water isotope ratio of precipitation (precipitation weighted,  
343  $\delta^{18}\text{O}_{\text{precip}}$ , Fig. 2a) over the ISM region during the JJAS season in the PI simulation is  
344  $-7\text{‰}$ . This is considerably more negative than the mean of  $-3.7\text{‰}$  calculated from the  
345 available GNIP observational data over the domain (Fig. 2a). A likely reason for the  
346 more negative  $\delta^{18}\text{O}_{\text{precip}}$  values simulated in the ISM region is the wet bias in the  
347 model (Fig. 1c) and consequent depletion of the heavier isotopes, as also suggested  
348 by previous studies using isotope-enabled CAM and iCESM models (Nusbaumer et  
349 al. 2017; Tharammal et al. 2017; Tharammal et al. 2023). It should be noted, however,  
350 that while the simulated domain-mean  $\delta^{18}\text{O}_{\text{precip}}$  shows a negative bias, the spatial pattern  
351 compares well with several GNIP stations across India. However, a lack of wider  
352 observational networks and continuous monitoring of seasonal  $\delta^{18}\text{O}_{\text{precip}}$  values  
353 hinder a comprehensive comparison of the observations and our simulation.  
354

355 In the PI simulation, the linear regression analysis between the JJAS mean  $\delta^{18}\text{O}_{\text{precip}}$   
356 values and the precipitation amount show a moderate amount effect in the ISM  
357 region ( $-0.22\text{‰}/\text{mm day}^{-1}$  slope of the spatial amount effect, the square of the

Deleted: It should be noted, h

Deleted: that

360 Pearson correlation coefficient  $r^2$  0.37, Fig. S3). The moderate strength of this  
361 relationship, which is physically related to rainout during heavy rainfall and  
362 convective events (Risi et al. 2008; [Lee and Fung 2008](#); [Tharammal et al. 2017](#)),  
363 suggests that factors other than local precipitation amount also strongly influence the  
364 simulated  $\delta^{18}\text{O}_{\text{precip}}$  values. These may include large-scale circulation, upstream  
365 convection, or the effects of water vapor sources with differing isotope signatures  
366 (Risi et al., 2008; [Pausata et al., 2011](#); Tharammal et al., 2023), as discussed in the  
367 following section.

Deleted: Tharammal et al.

Deleted: Pausata et al., 2011;

### 368 3.1.3 Water vapor sources and their effect on $\delta^{18}\text{O}_{\text{precip}}$ in the PI climate

369  
370 We used source water tagging to identify the primary water vapor sources for ISM  
371 precipitation in the PI simulation. Our simulation shows that the 17 tagged source  
372 regions (Fig. S2) contribute approximately 96% of the total JJAS precipitation (Fig.  
373 2b). Four major sources- the South Indian Ocean (SIO) and Central Indian Ocean-  
374 CIO (22% and 10% respectively), Arabian Sea (19%), and Indian land recycling  
375 (17%), together account for ~68% of the total precipitation. The Bay of Bengal (BOB)  
376 contributes only ~3% to the ISM precipitation. These results are consistent with  
377 previous water vapor tracking studies in the ISM domain using Lagrangian models  
378 (e.g. Gimeno et al. 2010, 2012; Ordóñez et al. 2012; Pathak et al. 2014; Dey and  
379 Döös 2021) and present-day results using the iCESM model (Tharammal et al.  
380 2023).

381  
382 The precipitation contribution-weighted sum of  $\delta^{18}\text{O}_{\text{pi}}$  of all the 17 tags at the sink (-  
383 6.7‰, based on Eqn. 4) explains ~95% of the domain mean  $\delta^{18}\text{O}_{\text{precip}}$  in the ISM  
384 region (-7‰, cf. 3.1.2), which validates our source-tagging framework (Eqn. 4, Fig.  
385 2c). The results show substantial differences in the isotope signatures between the  
386 major sources, mainly influenced by transport distance. For instance, while the  
387 Arabian Sea and SIO contribute comparably to JJAS precipitation (19% and 22%,  
388 respectively), their water isotopic signatures in precipitation ( $\delta^{18}\text{O}_{\text{pi}}$ ) greatly differ.  
389 The Arabian Sea source is relatively enriched (-0.1‰ mean over the ISM region),  
390 whereas the SIO has much depleted  $\delta^{18}\text{O}_{\text{pi}}$  values of -2.5‰ (Fig. 2c). This is likely  
391 due to the larger distance of the SIO source from the ISM sink region and  
392 consequent depletion of the vapor during condensation and rainouts in the path.

395 Similarly, the evapotranspiration from the ISM land domain, recycling source,  
396 contributes 17% to the total precipitation, and the  $\delta^{18}\text{O}_{\text{pi}}$  values of recycling are  
397 comparatively enriched (-0.6‰), likely due to being the local source of vapor. Hence,  
398 we suggest that the isotopic composition of ISM precipitation is sensitive to the  
399 relative contributions of these dominant water vapor sources and their isotopic  
400 signatures.

401

### 402 3.2 Global climate response in the LGM simulation

403 In the LGM simulation, the annual global mean surface temperature cooled by  
404 6.75°C compared to the PI (Fig. S4a). While this cooling is consistent with coupled  
405 CESM simulations (-6.8°C; Zhu et al. 2017; Tierney et al. 2020**b**), it is greater in  
406 magnitude than the PMIP4 multi-model mean (Kageyama et al. 2020). The cooling is  
407 more pronounced over the Laurentide ice sheets and in the polar regions, due to ice  
408 sheet albedo feedback and polar amplification. This leads to an asymmetry in the  
409 annual cooling between the two hemispheres, with Northern Hemisphere (NH)  
410 cooling (-7.5°C) exceeding that of the Southern Hemisphere (SH; -6.0°C)  
411 ( $\Delta\text{TS}=1.4^\circ\text{C}$ ). This interhemispheric asymmetry in cooling is smaller than previous  
412 modeling studies that found values more than 3°C (Broccoli, 2000). The simulated  
413 cooling in the high latitude ocean regions (~5 to 6°C, Fig. S1a) agrees well with the  
414 proxy-reconstructions (MARGO Project Members 2009). However, the model  
415 simulates colder SSTs in the tropics compared to the MARGO and GLOMAP  
416 reconstructions as noted by previous studies (~3°C in CESM simulations versus  
417 ~1.5°C; Tierney et al. 2020**b**).

418

419 Globally, the annual mean precipitation reduces by ~12% (Fig. S4b) in the LGM,  
420 consistent with proxy records and modeling studies including the PMIP4 LGM  
421 simulations (Bartlein et al. 2011; Yan et al. 2016; DiNezio et al. 2018; Kageyama et  
422 al. 2020). This reduction corresponds to a global hydrological sensitivity of ~1.8% per  
423 °C of cooling, and is close to the estimated thermodynamic increase in global  
424 precipitation of 2% per unit increase in temperature (Trenberth 2011). Despite the  
425 reduction in global mean precipitation, an increase in precipitation is simulated in

Deleted: (

427 some regions such as, tropical Pacific, parts of N. America, and South Africa, and  
428 these patterns are also found in the PMIP4 simulations (Kageyama et al. 2020).  
429  
430 Furthermore, we find that the position of the annual mean Intertropical Convergence  
431 Zone (ITCZ), defined as the median of zonal precipitation (20°S-20°N; McGee et al.  
432 2014; Devaraju et al. 2015), shifts northward by 1.2° in the LGM simulation. This  
433 finding contrasts with the southward shift of ITCZ in the LGM reported in many of the  
434 PMIP4 models (Wang et al. 2023), but is consistent with results from CESM2 (Zhu et  
435 al. 2022; Lofverstrom and Zhu 2023) as also reported in Wang et al. (2023).  
436 Lofverstrom and Zhu (2023) attribute this possible bias in the LGM ITCZ shift to  
437 biases in the CESM's cloud microphysics. It is likely that the simulated northward  
438 displacement of the ITCZ in the LGM in our simulation is due to a robust increase in  
439 precipitation over the northern tropical Pacific, coupled with widespread drying in the  
440 Southern Hemisphere tropical regions (Fig. S4b).

Deleted: model's

### 441 3.3 Indian summer monsoon precipitation during the LGM

442 The LGM simulation shows a substantial reduction in the Indian summer monsoon  
443 precipitation (Fig. 3), characterized by widespread drying over India, SE Asia, and  
444 Arabian Peninsula region. The precipitation amount is reduced by ~15% over the  
445 ISM domain, which is notable since a precipitation deficit exceeding 10% from the  
446 long-term mean is considered drought conditions in India (Shewale and Kumar  
447 2005). The ISM precipitation responses in the LGM simulation are broadly consistent  
448 with both monsoon proxy-records and previous climate model simulations (Jiang et  
449 al. 2015; Dutt et al., 2015; Yan et al. 2016; Kageyama et al. 2020). The large-scale  
450 drying is primarily due to regional and global cooling in both annual and summer  
451 means (Fig. S4a, S5a) and generally reduced evaporation from the tropical oceans  
452 (Fig. S5b). These patterns are linked to decreased atmospheric humidity and  
453 reduced column-integrated precipitable water (reduction of 25.2% over the ISM  
454 domain, Fig. S6). However, the drying during the summer monsoon season is not  
455 uniform across the region. Increased precipitation is simulated in the east part of  
456 India and the Bay of Bengal (Fig. 3). As this increase cannot be explained by the  
457 precipitable water anomalies in the LGM (Fig. S6), it is likely driven by changes in  
458 atmospheric circulation.

460 **3.3.1 Monsoon circulation changes in the LGM and moisture budget**

461 A regional intensification of the low-level westerly winds is simulated across the  
462 central and southern parts of India and the Bay of Bengal (Fig. 3, Fig. S7b). This  
463 regional intensification of the monsoon circulation is captured by several monsoon  
464 circulation indices used in this study- an increased vertical shear of zonal winds,  
465 strengthening of the Somali Jet, and enhanced barotropic shear (Fig. 4b, d, f,  
466 respectively). We suggest the enhanced westerly circulation in parts of the monsoon  
467 region, especially the Somali jet, is influenced by a stronger Mascarene high in the  
468 Southern Indian Ocean (Fig. 4e, S8b) that enhances the pressure gradient between  
469 the Indian land and the Southern Indian Ocean by ~2 mb (Fig. S8b, 4e). The  
470 strengthened Mascarene high is likely associated with the sea ice extension and  
471 cooling in the Southern Indian Ocean during the LGM (Fig. S1b, c). This agrees with  
472 the positive relationship between the ISM circulation and pressure gradient between  
473 the Indian monsoon region and the Mascarene high, suggested by several previous  
474 studies (Kripalani et al. 2007; Vidya et al. 2020; Azhar et al. 2023). However, the  
475 tropospheric temperature gradient ( $\Delta T T$ ), shows a weakening by 2.5% in the LGM.  
476 This indicates a weaker thermal forcing of the monsoon, likely due to enhanced  
477 cooling in the northern box used for the estimation of  $\Delta T T$  (Fig. S2b, S5a), in the  
478 LGM simulation.

479  
480 We also calculated corresponding monsoon indices from the coupled iCESM model  
481 results for the LGM and PI simulations (Fig. S9: Tierney et al. 2020b; Zhu and  
482 Poulsen, 2021). The coupled model results, except for  $\Delta T T$  index, are largely  
483 consistent with our fixed-SST iCESM simulations, with the indices indicating a  
484 strengthened Somali jet, enhanced barotropic shear, an intensified Mascarene High,  
485 reduced VIMT, and enhanced vertical shear of the zonal winds in the LGM  
486 simulation. The  $\Delta T T$  estimated from the coupled simulation shows an opposite  
487 response compared to the iCESM results, although the magnitude of the response in  
488 both is small (-2% in iCESM versus +5% in the coupled simulation).

489  
490 Although the strengthening of the westerlies dominates over most of the monsoon  
491 domain, a weakening of the low-level (850 hPa) westerly circulation and wind speeds  
492 towards land is simulated over the Northern Arabian Sea (Fig. 3, Fig. S7b). This is

Formatted: Font: 12 pt

Formatted: Font: Not Bold

Formatted: Normal

Deleted: The LGM simulation shows a weakening of the low-level (850 hPa) westerly circulation and wind speeds towards land over the Northern Arabian Sea (Fig. 3, Fig. S7b),

497 driven by substantially weakened land-ocean thermal (Fig. S5a, larger cooling over  
498 the land) and pressure gradients (S8b; Roxy et al. 2015; Weldeab et al. 2022).  
499 Surface cooling over the Indian subcontinent (domain mean  $-4.5^{\circ}\text{C}$ ; Table S2) in the  
500 LGM is approximately  $1^{\circ}\text{C}$  greater than the sea surface temperature cooling in the  
501 neighbouring Arabian Sea, which is consistent with the lower heat capacity of land,  
502 leading to more pronounced cooling and enhanced surface pressure over land.

503

504 The indices related to monsoon circulation (vertical shear of zonal winds, Somali jet  
505 speed index, pressure gradient between MH and ISM regions that characterize  
506 dynamical responses (Fig. 4)) show a general strengthening of the monsoon  
507 circulation by  $\sim 12\text{-}15\%$  in the LGM simulation, compared to the PI. The barotropic  
508 index shows an even larger percentage change between LGM and PI of  $>100\%$ .  
509 However, the index related to water vapor content and its transport (the monsoon  
510 hydrological index and Vertically Integrated Moisture Transport VIMT that  
511 characterize thermodynamical responses, (Fig. 4c, S10, Fasullo et al. 2003) shows a  
512 reduction by  $7.5\%$ , along with a reduction of column-integrated precipitable water  
513 over the ISM region by  $\sim 25\%$  (Fig. S6). This shows that the reduction in the ISM  
514 precipitation in the LGM simulation is mainly due to the thermodynamic response to  
515 the cooling (reduced water vapor in the atmosphere), despite an enhanced  
516 dynamical response (circulation changes).

517

518 To understand the drivers of the regional precipitation changes, we analysed the  
519 surface moisture budget (net precipitation, P-E), decomposing it into contributions  
520 from horizontal and vertical advection of moisture (Section 2.3, Chou and Lan,  
521 2012). The analysis (Fig. 5) shows that the drying over most parts of the ISM domain  
522 is primarily driven by the reduction in horizontal moisture advection (Fig. 5b),  
523 reflecting both reduced atmospheric humidity and weakened moisture transport.  
524 Further, the vertical advection term (Fig. 5c) also contributes to drying over north and  
525 west regions in India, indicating suppressed upward motion in this region. This is due  
526 to both the reduction in the moisture availability, and reduced transport as discussed  
527 before. In contrast, the increased precipitation in eastern part of India and BOB in the  
528 LGM is caused by enhanced moisture convergence and vertical advection (Fig. 5c)  
529 linked to the intensified monsoon westerlies in that region. We note that these results

**Deleted:** The circulation response is not uniform across the region, as a regional intensification of the low-level westerly winds is simulated across the central and southern parts of India and the Bay of Bengal (Fig. 3, Fig. S7b). This regional intensification of the monsoon circulation is captured by several monsoon circulation indices used in this study- an increased vertical shear of zonal winds, strengthening of the Somali Jet, and enhanced barotropic shear (Fig. S9b, d, f, respectively). We suggest the enhanced westerly circulation in parts of the monsoon region, especially the Somali jet, is influenced by a stronger Mascarene high in the Southern Indian Ocean (Fig. S9e, S8b) that enhances the pressure gradient between the Indian land and the Southern Indian Ocean by  $\sim 2$  mb (Fig. S8b, S9e). The strengthened Mascarene high is a result of the sea ice extension and cooling in the Southern Indian Ocean during the LGM (Fig. S1b, c). This is in agreement with the positive relationship between the ISM circulation and pressure gradient between the Indian monsoon region and the Mascarene high, suggested by several previous studies (Kripalani et al. 2007; P J et al. 2020; Azhar et al. 2023). However, the tropospheric temperature gradient ( $\Delta T T$ ), shows a weakening by  $2.5\%$  in the LGM. This indicates a weaker thermal forcing of the monsoon, likely due to enhanced cooling in the northern box used for the estimation of  $\Delta T T$  (Fig. S2b, S5a), in the LGM simulation.¶

¶ We note that t...

**Deleted:** S9

**Deleted:** S9c

**Deleted:** The analysis (Fig. 4) shows that the major term related to the drying (Fig. 4a) in the ISM region is the decrease in the horizontal moisture advection (Fig. 4b). ...

**Deleted:** 4c

568 for the advection terms include both dynamic and thermodynamic responses (Chou  
569 and Lan 2012) and delineating them is out of the scope of this paper.

570

571 The ISM precipitation reductions are also associated with large-scale zonal  
572 temperature gradients between a cold tropical western Pacific Ocean and a relatively  
573 colder Indian subcontinent (Fig. S5a). This leads to anomalous updrafts over the  
574 western Pacific, and increased subsidence over the Indian region (Fig. 6b, Fig.  
575 S11b, d). The relationship between a warmer W. Pacific and drying over the Indian  
576 region is discussed in previous studies (Annamalai et al. 2013). Furthermore, the  
577 Western tropical Pacific is ~1.5°C warmer compared to the Central and Eastern  
578 tropical Pacific in the LGM simulation (Fig. S5a). This intensifies the Pacific Walker  
579 circulation further, and enhances the subsidence and drying over the Eastern Pacific  
580 and the Indian subcontinent in the LGM. We suggest this large-scale circulation  
581 response enhanced the drying over India in the LGM simulation.

Deleted: 5

Deleted: ,

#### 582 3.4 Monsoon water vapor sources under glacial conditions

583 In the LGM simulation, the major four sources - SIO, Arabian Sea, recycling, and  
584 CIO- remain unchanged (23%, 21%, 19%, and 10% contributions to total  
585 precipitation, respectively) and their relative contributions change by less than 4%  
586 compared to the PI (Fig. 7b). However, the absolute amount of moisture from each  
587 source decreases by 10-14% (Fig. 7a). This reduction is primarily driven by reduced  
588 evaporative fluxes over the source regions (up to ~50% from the PI values; Fig. S5b,  
589 Table S2) and a general weakening of the moisture transport (Fig. S8b). The  
590 reduction in horizontal advection term over the ISM region in the moisture budget  
591 (Fig. 5b) corroborates with these results. This suggests that changes in atmospheric  
592 circulation and cooling of sea surface temperatures during the LGM significantly  
593 impacted the availability and transport of moisture to the Indian monsoon region.

Deleted: 6b

Deleted: 6a

Deleted: 4

#### 594 3.5 $\delta^{18}\text{O}_{\text{precip}}$ in the LGM

595 Globally, the LGM simulation shows a strong depletion in annual mean  $\delta^{18}\text{O}_{\text{precip}}$   
596 values (by 5 to >10‰) over the high latitudes and continental ice sheets (Fig. S4c).  
597 This is mainly due to the “temperature effect”, as the cooling in the LGM leads to a  
598 stronger Rayleigh distillation process (Galewsky et al. 2016). Previous studies

604 (Broccoli and Manabe 2008; Tharammal et al. 2013; [Kageyama et al. 2020](#); Zhu and  
605 Poulsen 2021) have shown that reduced GHG and consequent cooling, changes in  
606 circulation, and both topography and albedo of the ice sheets contribute to this  
607 depletion in the high latitudes. In the following text, we discuss the changes in  
608  $\delta^{18}\text{O}_{\text{precip}}$  over the ISM region during the JJAS season.

609

610 In contrast to the high latitudes, considerable enrichment of  $\delta^{18}\text{O}_{\text{precip}}$  (1‰-4‰) over  
611 tropical regions including the Indian Ocean, Southeast Asia, and ISM regions (mean  
612 enrichment of 0.9‰ over the ISM domain) is simulated in the JJAS season (Fig. 8).

613 This simulated enrichment is in agreement with the proxy data records from the  
614 South Asian summer monsoon region and climate model simulations (Hoffmann and  
615 Heimann 1997; Tiwari et al. 2011; Liu et al. 2014; Jiang et al. 2015; Kathayat et al.  
616 2016; Kaushal et al. 2018).

617

618 The JJAS mean amount effect in the LGM (spatial slope  $-0.24 \text{‰/mmd}^{-1}$ ,  $r^2=0.30$ ,  
619 Fig. S3) is moderate and similar to that in the PI simulation. Importantly, the linear  
620 regression analysis (Fig. S3) shows that there is no significant correlation between  
621 the changes in precipitation ( $\Delta P$ ) and the changes in  $\delta^{18}\text{O}_{\text{precip}}$  between the LGM and  
622 PI simulations (temporal slope of amount effect,  $\Delta\delta^{18}\text{O}_{\text{precip}}/\Delta P$ , slope  $-0.09$   
623  $\text{‰/mmd}^{-1}$ ,  $r^2=0.07$ ). Hence, the LGM enrichment in the ISM region cannot be  
624 explained by the amount effect, and the results indicate the influence of other factors  
625 such as changes in water vapor sources and atmospheric circulation.

626

### 627 **3.6 Drivers of monsoon $\delta^{18}\text{O}_{\text{precip}}$ changes: Perspectives from source tagging**

628 To diagnose the physical processes responsible for the changes in the monsoon  
629  $\delta^{18}\text{O}_{\text{precip}}$  during the LGM, we conducted a decomposition analysis of the JJAS mean  
630 LGM-PI  $\delta^{18}\text{O}_{\text{precip}}$  anomalies, following (Tabor et al. 2018). Details of the calculations  
631 are given in Section 2.4. Using the results from water tagging experiments, we  
632 separated the anomalies (LGM-PI) in the  $\delta^{18}\text{O}_{\text{precip}}$  of each source tag ( $\Delta\delta^{18}\text{O}_{\text{pi}}$ ) into  
633 4 components: 1) effects of changes in source vapor  $\delta^{18}\text{O}$  ( $\Delta\delta^{18}\text{O}_{\text{source}}$ ), 2) effects of  
634 changes in rainout during transport ( $\Delta\delta^{18}\text{O}_{\text{rainout}}$ ), 3) effects of changes during  
635 condensation over the Indian monsoon domain ( $\Delta\delta^{18}\text{O}_{\text{condensation}}$ ), and, 4) effects of

Deleted: ;

Deleted:

Deleted: Kageyama et al. 2020)

Deleted: 7

Deleted: in

641 changes in the relative contributions of each source to total precipitation over India  
642 (Shown in Fig. 9a-d).

Deleted: 8

643

644

645 The analysis shows that the dominant contributor to the positive anomalies in the  
646  $\delta^{18}\text{O}_{\text{precip}}$  values over the ISM domain is the change in the relative contribution of the  
647 water vapor sources, which accounts for an enrichment of +0.6‰ (Fig. 9d). This is  
648 caused by a reduction in the relative contribution from remote and depleted water  
649 vapor sources- North and South Pacific, Atlantic, and South China Sea (Fig. 9d).

Deleted: 8

Deleted: 8

650 The second largest positive contribution is from the Rainout Effect (+0.4‰ in total,  
651 Fig. 9b). This is driven by a weaker rainout along transport pathways from major

Deleted: 8

652 water vapor sources -Southern and Central Indian Ocean, due to a weaker  
653 circulation in many parts of the Indian Ocean, and overall reduced rainfall in the  
654 LGM. In contrast, the Source Effect (effects of changes in source vapor  $\delta^{18}\text{O}$ , Fig.

655 9a) provides a small net negative contribution, as a positive contribution from the

Deleted: 8

656 Arabian Sea is offset by negative effects from other source regions (Fig. 9a). The

Deleted: 8

657 positive effect from the Arabian Sea source is likely due to a localized increase in  
658 evaporation (Fig. S5b) in contrast to other sources where evaporation was generally  
659 reduced, and also the prescribed 1‰ global ocean surface enrichment in the LGM  
660 simulation.

661

662 The condensation term, which represents the local enrichment of the precipitation at  
663 the sink during the phase transition of vapor to precipitation, produces a negative net

Deleted: only

664 contribution (Fig. 9c). This suggests that the isotopic enrichment of precipitation on  
665 condensation was weaker in the LGM compared to the PI. This finding also confirms

Deleted: minor and slightly

Deleted: 8

666 that the amount effect is not a primary driver of the LGM enrichment. If a strong  
667 amount effect existed, the reduced LGM precipitation should have produced a  
668 positive condensation term. The negative contribution from the condensation term,  
669 therefore, agrees with our previous analysis showing no significant temporal  
670 correlation between changes in ISM precipitation and isotopes (Section 3.5; Figure

671 S3) in the LGM. The condensation term in our framework reflects the isotopic

672 enrichment in precipitation relative to ambient vapor. A negative response for the

673 effect suggests a weaker enrichment during condensation in the LGM, likely related

674 to reduced convection and condensation, also potentially lower fractionation

684 efficiency under the cooler and drier LGM conditions. Furthermore, cold conditions  
685 can reduce re-evaporation of precipitation (Worden et al. 2007), a process that  
686 usually leads to a more isotope enriched precipitation. However, these aspects  
687 warrant further investigation in future studies.

#### 688 4. Discussion and Conclusions

689 The present study used a water isotope, water tagging-enabled general circulation  
690 model to investigate the Indian summer monsoon precipitation and isotope  
691 responses under glacial conditions. Our simulations show a 15% reduction of  
692 monsoon precipitation over the Indian domain. Our study shows that the reduction in  
693 Indian monsoon precipitation is mainly due to the effects of global cooling and  
694 reduced humidity (due to reduced CO<sub>2</sub> and the presence of continental ice-sheets;  
695 (Kageyama et al. 2020), The LGM drying over the Indian subcontinent was  
696 enhanced by a Walker-like circulation response, driven by zonal temperature  
697 gradients between the less-cooled Western Pacific and the cooler Indian  
698 subcontinent, which created anomalous subsidence over the Indian region.

699 The reduction in the summer monsoon precipitation in the LGM simulation is  
700 consistent with climate models and proxy records of monsoon precipitation (Liu et al.  
701 2021; Jiang et al. 2015; Wang et al. 2023; Yan et al. 2016; Cao et al. 2019). The  
702 simulated northward shift of the ITCZ in our iCESM results, likely due to increased  
703 tropical North Pacific precipitation, conflicts with the southward shift simulated by  
704 several other models (Wang et al. 2023). This discrepancy points to uncertainties in  
705 climate simulations and suggests that more studies are required to assess the  
706 representation of tropical ocean-atmosphere interactions under the glacial climate  
707 conditions.

708 We also note that the low-level circulation responses in the LGM simulation  
709 (enhanced cyclonic barotropic shear with enhanced westerly anomalies over  
710 Southern India, and easterlies over the northern latitudes) is consistent with the  
711 climate model responses in future warming scenarios (Menon et al. 2013). Menon et  
712 al. (2013) find that under the RCP8.5 scenario, CMIP5 models project a weaker low  
713 level cyclonic monsoon circulation with enhanced westerly anomaly over northern

Deleted: , and a weakened land-ocean temperature gradient which reduced the strength of the monsoonal circulation in many parts of the ISM region

717 India and easterly anomaly over the south, despite a simulated increase in the  
718 monsoon precipitation. Thus, our results are consistent with monsoon responses in  
719 future warming scenarios, such that in the colder LGM conditions, the monsoon  
720 precipitation is reduced due to thermodynamic response to cooling, while the  
721 dynamical response characterized by monsoon circulation indices in general is  
722 intensified.

723 A key contribution of this study is the novel application of water vapor source-  
724 tagging to the LGM climate simulation, which shows that the major water vapor  
725 sources for the Indian monsoon were unchanged between the pre-industrial and  
726 LGM climates. Our study finds that isotopic ratio of precipitation is enriched by  $\sim 1\text{‰}$   
727 over the ISM domain during the LGM, which is in agreement with speleothem proxy  
728 records from Mawmluh (Dutt et al. 2015) and Bittoo caves (Kathayat et al. 2016) in  
729 North India. Our analysis confirms the amount effect (Dansgaard 1964) was not the  
730 primary driver for this enrichment, as we find no significant correlation between the  
731 changes in precipitation and  $\delta^{18}\text{O}_{\text{precip}}$  from the PI to the LGM. Instead, our  
732 decomposition analysis using water vapor tagging finds that the simulated LGM  
733 enrichment is due to a reduced relative contribution from distant, isotopically  
734 depleted moisture sources and decreased rainout from Indian Ocean sources. A key  
735 component of the enrichment in  $\delta^{18}\text{O}_{\text{precip}}$  is the reduction in Pacific moisture  
736 contribution in the LGM, which is highly isotopically depleted. Our decomposition  
737 analysis shows that the reduction in the relative contribution from the North Pacific  
738 alone contributes approximately  $+0.4\text{‰}$  enrichment (Fig. 9d). This reduced Pacific  
739 moisture contribution also reflects the circulation response in the LGM. The  
740 enhanced Walker-like circulation, together with the enhanced westerlies intensify  
741 convection over the western Pacific and weaken moisture transport from the  
742 Northern Pacific into South Asia.

743 The results are in agreement with studies by Tabor et al. (2018) and Hu et al. (2019)  
744 who find the importance of different water vapor sources for the South Asian and  
745 East Asian monsoon  $\delta^{18}\text{O}_{\text{precip}}$  values. Our results imply that  $\delta^{18}\text{O}$  changes recorded  
746 in speleothems and marine sediments from the Indian monsoon region during the  
747 LGM should be interpreted primarily as indicators of changes in moisture sources  
748 and their relative contributions and large-scale circulation, rather than as direct

Deleted: S

Deleted:

Deleted: Hence, this study emphasizes that rather than being a simple proxy for local rainfall, the  $\delta^{18}\text{O}_{\text{precip}}$  values in the ISM region is a complex signal integrating large-scale atmospheric dynamics and moisture sources. Further, these findings pose questions for the interpretation of paleoclimate records where  $\delta^{18}\text{O}$  values of climate records are used as a direct proxy for local precipitation intensity.

759 proxies for local monsoon precipitation intensity. We suggest  $\delta^{18}\text{O}$  in paleoclimate  
760 archives is better considered as an integrated representation of changes in  
761 hydrological cycle, rather than a direct measure of local rainfall amount. This also  
762 shows that combining proxy archives with isotope-enabled climate model simulations  
763 is crucial for accurately interpreting past monsoon changes.

764 We note that our study has a few limitations. The version of the CESM model we  
765 used has high climate sensitivity and overestimates the LGM global cooling (Zhu et  
766 al. 2022), an issue attributed to its cloud parameterization. However, we suggest that  
767 these biases do not affect our key results, as the model is able to both successfully  
768 capture the present-day monsoon circulation, and isotopic distribution. The model is  
769 also able to simulate the isotopic enrichment found in proxy records during the LGM.  
770 Further, we use a single model, with prescribed SSTs and prescribed surface ocean  
771 water isotope ratios because of the cost of computation when we utilize the water-  
772 tagging capabilities of the model. Future work should employ fully coupled Earth  
773 system models within a multi-model framework to investigate ocean-atmosphere-  
774 isotope feedback and test the robustness of these results.

775 In conclusion, this study disentangles the drivers of Indian monsoon precipitation and  
776 its isotopic signature during the LGM. The results highlight that the isotopic  
777 composition of precipitation in the Indian monsoon region is a complex signal  
778 integrating changes in circulation, changes in relative contribution of water vapor  
779 sources, and upstream rainout processes. These findings underscore the importance  
780 of considering moisture source and transport history when interpreting paleoclimate  
781 isotope records from the Indian monsoon and other tropical monsoon regions.

#### 782 **Code/Data availability**

783 The datasets used in the current study will be made available to the public.

#### 784 **Author contributions**

785 TT: Conceptualization, Funding acquisition, Methodology, Investigation, Formal  
786 analysis, Visualization, Writing - Original Draft. GB: Methodology, Analysis, Writing -

787 Review & Editing. JN: Methodology, Model software, Analysis, Writing - Review &  
788 Editing.

789 **Competing interests**

790 None of the authors has any competing interests.

791 **Acknowledgements**

792 TT is supported by the DST-INSPIRE Faculty Fellowship awarded by the  
793 Department of Science and Technology, India and Anusandhan National Research  
794 Foundation (ANRF) Early Career Research Grant. We acknowledge Jiang Zhu  
795 (NCAR) for providing the boundary conditions for the simulations, and we would like  
796 to thank Dr. André Paul for discussions during the initial stages of this research. We  
797 acknowledge the high-performance computing support from the Supercomputer  
798 Education and Research Centre (SERC), Indian Institute of Science, Bangalore. All  
799 the figures in the manuscript were created with NCL (NCAR Command Language  
800 Version 6.6.2, <http://www.ncl.ucar.edu/>).

801 **References:**

- 802 Adler, R. F., M. Sapiano, G. J. Huffman, J. Wang, G. Gu, D. Bolvin, L. Chiu, et al.  
803 2018. "The Global Precipitation Climatology Project (GPCP) Monthly Analysis  
804 (New Version 2.3) and a Review of 2017 Global Precipitation." *Atmosphere* 9  
805 (4). <https://doi.org/10.3390/atmos9040138>.
- 806 Annamalai, H., Jan Hafner, K. P. Sooraj, and P. Pillai. 2013. "Global Warming Shifts  
807 the Monsoon Circulation, Drying South Asia." *Journal of Climate* 26 (9): 2701–  
808 18.
- 809 Azhar, Siti Syairah Atiqah, Sheeba Nettukandy Chenoli, Azizan Abu Samah, Seong-  
810 Joong Kim, and Nuncio Murukesh. 2023. "The Mechanism Linking the Variability  
811 of the Antarctic Sea Ice Extent in the Indian Ocean Sector to Indian Summer  
812 Monsoon Rainfall." *Climate Dynamics* 60 (9-10): 2665–85.
- 813 Bartlein, P. J., S. P. Harrison, S. Brewer, S. Connor, B. A. S. Davis, K. Gajewski, J.  
814 Guiot, et al. 2011. "Pollen-Based Continental Climate Reconstructions at 6 and  
815 21 Ka: A Global Synthesis." *Climate Dynamics* 37 (3-4): 775–802.

816 Bailey, Adriana, David Noone, Sylvia G. Dee, Jesse Nusbaumer, Jessica L. Conroy,  
817 Samantha Stevenson, and Alyssa Atwood. "Toward a process-oriented  
818 understanding of water in the climate system: recent insights from stable  
819 isotopes." *Environmental Research: Climate* (2024).

820 Boos, William R., and Kerry A. Emanuel. 2009. "Annual Intensification of the Somali  
821 Jet in a Quasi-equilibrium Framework: Observational Composites." *Quarterly  
822 Journal of the Royal Meteorological Society. Royal Meteorological Society  
823 (Great Britain)* 135 (639): 319–35.

824 Brady, E., S. Stevenson, D. Bailey, and Z. Liu. 2019. "The Connected Isotopic Water  
825 Cycle in the Community Earth System Model Version 1." *Journal of Advances*.  
826 <https://agupubs.onlinelibrary.wiley.com/doi/abs/10.1029/2019MS001663>.

827 Breitenbach, Sebastian F. M., Jess F. Adkins, Hanno Meyer, Norbert Marwan,  
828 Kanikicharla Krishna Kumar, and Gerald H. Haug. 2010. "Strong Influence of  
829 Water Vapor Source Dynamics on Stable Isotopes in Precipitation Observed in  
830 Southern Meghalaya, NE India." *Earth and Planetary Science Letters* 292 (1):  
831 212–20.

832 Broccoli, A. J., and S. Manabe. "The influence of continental ice, atmospheric CO<sub>2</sub>,  
833 and land albedo on the climate of the last glacial maximum." *Climate dynamics*  
834 1, no. 2 (1987): 87-99.

835 Broccoli, A. J., and S. Manabe. 2008. "The effects of the Laurentide ice sheet on  
836 North American climate during the last glacial maximum." *Géographie physique  
837 et quaternaire* 41 (2): 291–99.

838 Brovkin, Victor, Edward Brook, John W. Williams, Sebastian Bathiany, Timothy M.  
839 Lenton, Michael Barton, Robert M. DeConto, et al. 2021. "Past Abrupt Changes,  
840 Tipping Points and Cascading Impacts in the Earth System." *Nature Geoscience*  
841 14 (8): 550–58.

842 Cao, Jian, Bin Wang, and Libin Ma. 2019. "Attribution of Global Monsoon Response  
843 to the Last Glacial Maximum Forcings." *Journal of Climate* 32 (19): 6589–6605.

844 Chakraborty, Supriyo, Aharna Sarkar, Amey Datye, V. Praveen, Prमित Kumar Deb  
845 Burman, Yashas Shivamurthy, Nibedita Samal et al. "Precipitation isotopes and  
846 monsoon dynamics in the core monsoon zone of India." *Scientific Reports* 15,  
847 no. 1 (2025): 6761.

848 Chen, Ziming, Tianjun Zhou, Lixia Zhang, Xiaolong Chen, Wenxia Zhang, and Jie  
849 Jiang. 2020. "Global Land Monsoon Precipitation Changes in CMIP6

850 Projections." *Geophysical Research Letters* 47 (14).  
851 <https://doi.org/10.1029/2019gl086902>.

852 Chou, Chia, and Chia-Wei Lan. 2012. "Changes in the Annual Range of Precipitation  
853 under Global Warming." *Journal of Climate* 25 (1): 222–35.

854 Chou, Chia, J. David Neelin, Chao-An Chen, and Jien-Yi Tu. 2009. "Evaluating the  
855 'rich-Get-Richer' Mechanism in Tropical Precipitation Change under Global  
856 Warming." *Journal of Climate* 22 (8): 1982–2005.

857 Contreras-Rosales, L. A., and T. Jennerjahn. 2014. "Evolution of the Indian Summer  
858 Monsoon and Terrestrial Vegetation in the Bengal Region during the Past 18  
859 Ka." *Quaternary Science Reviews*.  
860 [https://www.sciencedirect.com/science/article/pii/S0277379114003242?casa\\_to](https://www.sciencedirect.com/science/article/pii/S0277379114003242?casa_to)  
861 [ken=aiCf2W3kwWoAAAAA:RuWH7AnsDqErlfnmonRPsagJObV6-](https://www.sciencedirect.com/science/article/pii/S0277379114003242?casa_to)  
862 [9b9whwrVSr6rj7yPvRiVPyzf-7c3hwkc1qzyjF1fdu52zu0](https://www.sciencedirect.com/science/article/pii/S0277379114003242?casa_to).

863 Dansgaard, W. 1964. "Stable Isotopes in Precipitation." *Tell'Us* 16 (4): 436–68.

864 Dee, Sylvia, Adriana Bailey, Jessica L. Conroy, Alyssa Atwood, Samantha  
865 Stevenson, Jesse Nusbaumer, and David Noone. 2023. "Water Isotopes,  
866 Climate Variability, and the Hydrological Cycle: Recent Advances and New  
867 Frontiers." *Environmental Research: Climate* 2 (2): 022002.

868 Devaraju, N., Govindasamy Bala, and Angshuman Modak. 2015. "Effects of Large-  
869 Scale Deforestation on Precipitation in the Monsoon Regions: Remote versus  
870 Local Effects." *Proceedings of the National Academy of Sciences of the United*  
871 *States of America* 112 (11): 3257–62.

872 Dey, Dipanjan, and Kristofer Döös. 2021. "Tracing the Origin of the South Asian  
873 Summer Monsoon Precipitation and Its Variability Using a Novel Lagrangian  
874 Framework." *Journal of Climate* 34 (21): 8655–68.

875 DiNezio, Pedro N., Jessica E. Tierney, Bette L. Otto-Bliesner, Axel Timmermann,  
876 Tripti Bhattacharya, Nan Rosenbloom, and Esther Brady. 2018. "Glacial  
877 Changes in Tropical Climate Amplified by the Indian Ocean." *Science Advances*  
878 4 (12): eaat9658.

879 Duplessy, Jean-Claude, Laurent Labeyrie, and Claire Waelbroeck. 2002.  
880 "Constraints on the Ocean Oxygen Isotopic Enrichment between the Last  
881 Glacial Maximum and the Holocene: Paleoceanographic Implications."  
882 *Quaternary Science Reviews* 21 (1-3): 315–30.

883 Dutt, Som, Anil K. Gupta, Steven C. Clemens, Hai Cheng, Raj K. Singh, Gayatri

884 Kathayat, and R. Lawrence Edwards. 2015. "Abrupt Changes in Indian Summer  
885 Monsoon Strength during 33,800 to 5500 Years B.P." *Geophysical Research*  
886 *Letters* 42 (13): 5526–32.

887 Fasullo, J., and P. J. Webster. 2003. "A Hydrological Definition of Indian Monsoon  
888 Onset and Withdrawal." *Journal of Climate* 16 (19): 3200–3211.

889 Gadgil, Sulochana. 2003. "The Indian Monsoon and Its Variability." *Annual Review of*  
890 *Earth and Planetary Sciences* 31 (1): 429–67.

891 Galewsky, Joseph, Hans Christian Steen-Larsen, Robert D. Field, John Worden,  
892 Camille Risi, and Matthias Schneider. 2016. "Stable Isotopes in Atmospheric  
893 Water Vapor and Applications to the Hydrologic Cycle." *Reviews of Geophysics*  
894 54 (4): 809–65.

895 Geen, Ruth, Simona Bordoni, David S. Battisti, and Katrina Hui. 2020. "Monsoons,  
896 ITCZs, and the Concept of the Global Monsoon." *Reviews of Geophysics* 58  
897 (4). <https://doi.org/10.1029/2020rg000700>.

898 Gimeno, Luis, Anita Drumond, Raquel Nieto, Ricardo M. Trigo, and Andreas Stohl.  
899 2010. "On the Origin of Continental Precipitation." *Geophysical Research Letters*  
900 37 (13). <https://doi.org/10.1029/2010gl043712>.

901 Gimeno, Luis, Andreas Stohl, Ricardo M. Trigo, Francina Dominguez, Kei  
902 Yoshimura, Lisan Yu, Anita Drumond, Ana María Durán-Quesada, and Raquel  
903 Nieto. 2012. "Oceanic and Terrestrial Sources of Continental Precipitation."  
904 *Reviews of Geophysics* 50 (4). <https://doi.org/10.1029/2012rg000389>.

905 Hanf, Franziska S., and H. Annamalai. 2020. "Systematic Errors in South Asian  
906 Monsoon Precipitation: Process-Based Diagnostics and Sensitivity to  
907 Entrainment in NCAR Models." *Journal of Climate* 33 (7): 2817–40.

908 He, C., Z. Liu, B. L. Otto-Bliesner, E. C. Brady, C. Zhu, R. Tomas, P. U. Clark, et al.  
909 2021. "Hydroclimate Footprint of Pan-Asian Monsoon Water Isotope during the  
910 Last Deglaciation." *Science Advances* 7 (4).  
911 <https://doi.org/10.1126/sciadv.abe2611>.

912 Hoffmann, G., and M. Heimann. 1997. "Water Isotope Modeling in the Asian  
913 Monsoon Region." *Quaternary International* 37:115–28.

914 Hu, Jun, Julien Emile-Geay, Clay Tabor, Jesse Nusbaumer, and Judson Partin.  
915 2019. "Deciphering Oxygen Isotope Records from Chinese Speleothems with an  
916 Isotope-enabled Climate Model." *Paleoceanography and Paleoclimatology* 34  
917 (12): 2098–2112.

918 Jiang, Dabang, Zhiping Tian, Xianmei Lang, Masa Kageyama, and Gilles Ramstein.  
919 2015. "The Concept of Global Monsoon Applied to the Last Glacial Maximum: A  
920 Multi-Model Analysis." *Quaternary Science Reviews* 126 (October):126–39.

921 Kageyama, Masa, Pascale Braconnot, Cristiano M. Chiessi, Kira Rehfeld, Yassine  
922 Ait Brahim, Marina Dütsch, Benjamin Gwinneth, et al. 2024. "Lessons from  
923 Paleoclimates for Recent and Future Climate Change: Opportunities and  
924 Insights." *Frontiers in Climate* 6 (December).  
925 <https://doi.org/10.3389/fclim.2024.1511997>.

926 Kageyama, Masa, and PMIP4 LGM group. 2020. "The PMIP4-CMIP6 Last Glacial  
927 Maximum Experiments: Preliminary Results and Comparison with the PMIP3-  
928 CMIP5 Simulations." <https://doi.org/10.5194/egusphere-egu2020-11153>.

929 Kathayat, Gayatri, Hai Cheng, Ashish Sinha, Christoph Spötl, R. Lawrence Edwards,  
930 Haiwei Zhang, Xianglei Li, et al. 2016. "Indian Monsoon Variability on Millennial-  
931 Orbital Timescales." *Scientific Reports* 6 (April):24374.

932 Kathayat, Gayatri, Ashish Sinha, Masahiro Tanoue, Kei Yoshimura, Hanying Li,  
933 Haiwei Zhang, and Hai Cheng. 2021. "Interannual Oxygen Isotope Variability in  
934 Indian Summer Monsoon Precipitation Reflects Changes in Moisture Sources."  
935 *Communications Earth & Environment* 2 (1): 1–10.

936 Katzenberger, Anja, Jacob Schewe, Julia Pongratz, and Anders Levermann. 2021.  
937 "Robust Increase of Indian Monsoon Rainfall and Its Variability under Future  
938 Warming in CMIP6 Models." *Earth System Dynamics* 12 (2): 367–86.

939 Kaushal, N., S. Breitenbach, F. Lechleitner, A. Sinha, V. Tewari, S. M. Ahmad, M.  
940 Berkelhammer, et al. 2018. "The Indian Summer Monsoon from a Speleothem  
941  $\delta^{18}\text{O}$  perspective—A Review." *Quaternary*, September.  
942 <https://doi.org/10.3390/QUAT1030029>.

943 K. Mukherjee, Sumit, Ayantika Dey Choudhury, and Raghavan Krishnan. 2024.  
944 "Heavy-Precipitating Mid-Tropospheric Cyclonic Systems of the Indian Summer  
945 Monsoon in a Warming Climate." <https://doi.org/10.5194/egusphere-egu24-268>.

946 Konecky, B. L., D. C. Noone, and K. M. Cobb. "The influence of competing  
947 hydroclimate processes on stable isotope ratios in tropical rainfall." *Geophysical  
948 Research Letters* 46, no. 3 (2019): 1622-1633.

949 Kong, Yunqi, Yuting Wu, Xiaoming Hu, Yana Li, and Song Yang. 2022. "Uncertainty  
950 in Projections of the South Asian Summer Monsoon under Global Warming by  
951 CMIP6 Models: Role of Tropospheric Meridional Thermal Contrast."

952        *Atmospheric and Oceanic Science Letters* 15 (1): 100145.

953 Kripalani, R. H., J. H. Oh, A. Kulkarni, S. S. Sabade, and H. S. Chaudhari. 2007.

954        “South Asian Summer Monsoon Precipitation Variability: Coupled Climate Model

955        Simulations and Projections under IPCC AR4.” *Theoretical and Applied*

956        *Climatology* 90 (3-4): 133–59.

957 Krishnan, R., T. P. Sabin, R. Vellore, M. Mujumdar, J. Sanjay, B. N. Goswami, F.

958        Hourdin, J-L Dufresne, and P. Terray. 2016. “Deciphering the Desiccation Trend

959        of the South Asian Monsoon Hydroclimate in a Warming World.” *Climate*

960        *Dynamics* 47 (3-4): 1007–27.

961 Krishnan, R., J. Sanjay, Chellappan Gnanaseelan, Milind Mujumdar, Ashwini

962        Kulkarni, and Supriyo Chakraborty. 2020. “Assessment of Climate Change over

963        the Indian Region: A Report of the Ministry of Earth Sciences (MOES),

964        Government of India,” 226.

965 Lambeck, K. 2000. “Global Ice Volumes at the Last Glacial Maximum and Early

966        Lateglacial.” *Earth and Planetary Science Letters* 181 (4): 513–27.

967 Lambeck, Kurt, Hélène Rouby, Anthony Purcell, Yiyang Sun, and Malcolm

968        Sambridge. 2014. “Sea Level and Global Ice Volumes from the Last Glacial

969        Maximum to the Holocene.” *Proceedings of the National Academy of Sciences*

970        *of the United States of America* 111 (43): 15296–303.

971 Lee, Jung-Eun, and Inez Fung. 2008. “‘Amount Effect’ of Water Isotopes and

972        Quantitative Analysis of Post-Condensation Processes.” *Hydrological Processes*

973        22 (1): 1–8.

974 LeGrande, A. N., and G. A. Schmidt. 2006. “Global Gridded Data Set of the Oxygen

975        Isotopic Composition in Seawater.” *Geophysical Research Letters* 12 (33).

976        <https://doi.org/10.1029/2006GL026011>.

977 Lewis, S. C., A. N. LeGrande, M. Kelley, and G. A. Schmidt. 2010. “Water Vapour

978        Source Impacts on Oxygen Isotope Variability in Tropical Precipitation during

979        Heinrich Events.” *Climate of the Past* 6 (3): 325–43.

980 Liu, Shengfa, Wenxing Ye, Min-Te Chen, Hui-Juan Pan, Peng Cao, Hui Zhang,

981        Somkiat Khokiattiwong, Narumol Kornkanitnan, and Xuefa Shi. 2021.

982        “Millennial-Scale Variability of Indian Summer Monsoon during the Last 42 Kyr:

983        Evidence Based on Foraminiferal Mg/Ca and Oxygen Isotope Records from the

984        Central Bay of Bengal.” *Palaeogeography, Palaeoclimatology, Palaeoecology*

985        562 (January):110112.

986 Liu, Z., X. Wen, E. C. Brady, B. Otto-Bliesner, and G. Yu. 2014. "Chinese Cave  
987 Records and the East Asia Summer Monsoon." *Quaternary Science Reviews*.  
988 [https://www.sciencedirect.com/science/article/pii/S0277379113004150?casa\\_to](https://www.sciencedirect.com/science/article/pii/S0277379113004150?casa_to)  
989 [ken=8RYar31ITq8AAAAA:vX8ZUyWAR\\_oJN\\_4Qie3b5WlxdKkgm1q\\_SpDVIUS-](https://www.sciencedirect.com/science/article/pii/S0277379113004150?casa_to)  
990 [cXBN0-6aFKZRgfLTYitdt9ljs5naycMenuqt.](https://www.sciencedirect.com/science/article/pii/S0277379113004150?casa_to)

991 Li, Xiuping, Lei Wang, Shiyuan Zhong, and Liu Liu. 2024. "Comparative Analysis of  
992 Indices in Capturing the Onset and Withdrawal of the South Asian Summer  
993 Monsoon." *Environmental Research Communications* 6 (3): 031007.

994 Lohmann, Gerrit, Martin Butzin, Nina Eissner, Xiaoxu Shi, and Christian Stepanek.  
995 "Abrupt climate and weather changes across time scales." *Paleoceanography*  
996 *and Paleoclimatology* 35, no. 9 (2020): e2019PA003782.

997 Lofverstrom, Marcus, and Jiang Zhu. 2023. "Tropical Precipitation Woes in the  
998 Community Earth System Model Version 2." *Geophysical Research Letters* 50  
999 (21). <https://doi.org/10.1029/2023gl104416>.

1000 Maher, B. A. 2008. "Holocene Variability of the East Asian Summer Monsoon from  
1001 Chinese Cave Records: A Re-Assessment." *Holocene* 18 (6): 861–66.

1002 MARGO Project Members. 2009. "Constraints on the Magnitude and Patterns of  
1003 Ocean Cooling at the Last Glacial Maximum." *Nature Geoscience* 2 (2): 127–32.

1004 McGee, David. "Glacial–interglacial precipitation changes." *Annual Review of Marine*  
1005 *Science* 12, no. 1 (2020): 525–557.

1006 McGee, David, Aaron Donohoe, John Marshall, and David Ferreira. 2014. "Changes  
1007 in ITCZ Location and Cross-Equatorial Heat Transport at the Last Glacial  
1008 Maximum, Heinrich Stadial 1, and the Mid-Holocene." *Earth and Planetary*  
1009 *Science Letters* 390 (March):69–79.

1010 Nusbaumer, J., T. E. Wong, and C. Bardeen. 2017. "Evaluating Hydrological  
1011 Processes in the Community Atmosphere Model Version 5 (CAM5) Using  
1012 Stable Isotope Ratios of Water." *Journal of Advances in*.  
1013 <https://agupubs.onlinelibrary.wiley.com/doi/abs/10.1002/2016MS000839>.

1014 Ordóñez, Paulina, Pedro Ribera, David Gallego, and Cristina Peña-Ortiz. 2012.  
1015 "Major Moisture Sources for Western and Southern India and Their Role on  
1016 Synoptic-Scale Rainfall Events." *Hydrological Processes* 26 (25): 3886–95.

1017 Pathak, Amey, Subimal Ghosh, and Praveen Kumar. 2014. "Precipitation Recycling  
1018 in the Indian Subcontinent during Summer Monsoon." *Journal of*  
1019 *Hydrometeorology* 15 (5): 2050–66.

- 1020 Pathak, Raju, Sandeep Sahany, Saroj Kanta Mishra, and S. K. Dash. 2019.  
1021 "Precipitation Biases in CMIP5 Models over the South Asian Region." *Scientific*  
1022 *Reports* 9 (1): 9589.
- 1023 Pausata, Francesco S. R., David S. Battisti, Kerim H. Nisancioglu, and Cecilia M.  
1024 Bitz. 2011. "Chinese Stalagmite  $\delta^{18}\text{O}$  Controlled by Changes in the Indian  
1025 Monsoon during a Simulated Heinrich Event." *Nature Geoscience* 4 (7): 474–80.
- 1026 Peltier, W. R., D. F. Argus, and R. Drummond. 2015. "Space Geodesy Constrains  
1027 Ice Age Terminal Deglaciation: The Global ICE-6G\_C (VM5a) Model." *Journal of*  
1028 *Geophysical Research. Solid Earth* 120 (1): 450–87.
- 1029 Rehfeld, Kira, Raphaël Hébert, Juan M. Lora, Marcus Lofverstrom, and Chris M.  
1030 Brierley. "Variability of surface climate in simulations of past and future." *Earth*  
1031 *System Dynamics* 11, no. 2 (2020): 447-468.
- 1032 Risi, Camille, Sandrine Bony, and Françoise Vimeux. 2008. "Influence of Convective  
1033 Processes on the Isotopic Composition ( $\delta^{18}\text{O}$  and  $\delta\text{D}$ ) of Precipitation and Water  
1034 Vapor in the Tropics: 2. Physical Interpretation of the Amount Effect." *Journal of*  
1035 *Geophysical Research*. <https://doi.org/10.1029/2008jd009943>.
- 1036 Roxy, Mathew Koll, Kapoor Ritika, Pascal Terray, Raghu Murtugudde, Karumuri  
1037 Ashok, and B. N. Goswami. 2015. "Drying of Indian Subcontinent by Rapid  
1038 Indian Ocean Warming and a Weakening Land-Sea Thermal Gradient." *Nature*  
1039 *Communications* 6 (1): 1–10.
- 1040 Seltzer, A. M., P. W. Davidson, S. A. Shackleton, D. P. Nicholson, and S. Khatiwala.  
1041 2024. "Global Ocean Cooling of 2.3°C during the Last Glacial Maximum."  
1042 *Geophysical Research Letters* 51 (9). <https://doi.org/10.1029/2024gl108866>.
- 1043 Shewale, M. P., and Shravan Kumar. 2005. "CLIMATOLOGICAL FEATURES OF  
1044 DROUGHT INCIDENCES IN INDIA."  
1045 <https://imdpune.gov.in/Reports/drought.pdf>.
- 1046 Sima, Adriana, André Paul, Michael Schulz, and Johannes Oerlemans. 2006.  
1047 "Modeling the Oxygen-Isotopic Composition of the North American Ice Sheet  
1048 and Its Effect on the Isotopic Composition of the Ocean during the Last Glacial  
1049 Cycle." *Geophysical Research Letters* 33 (15).  
1050 <https://doi.org/10.1029/2006gl026923>.
- 1051 Sinha, Ashish, Gayatri Kathayat, Hai Cheng, Sebastian F. M. Breitenbach, Max  
1052 Berkelhammer, Manfred Mudelsee, Jayant Biswas, and R. L. Edwards. 2015.  
1053 "Trends and Oscillations in the Indian Summer Monsoon Rainfall over the Last

Moved down [1]: P J, Vidya, M. Ravichandran, M. P. Subeesh, Sourav Chatterjee, and Nuncio M. 2020. "Global Warming Hiatus Contributed Weakening of the Mascarene High in the Southern Indian Ocean." *Scientific Reports* 10 (1): 3255. [1](#)

- 1062 Two Millennia." *Nature Communications* 6 (February):6309.
- 1063 Sjolte, Jesper, and Georg Hoffmann. 2014. "Modelling Stable Water Isotopes in  
1064 Monsoon Precipitation during the Previous Interglacial." *Quaternary Science  
1065 Reviews* 85 (February):119–35.
- 1066 Tabor, Clay R., Bette L. Otto-Bliesner, Esther C. Brady, Jesse Nusbaumer, Jiang  
1067 Zhu, Michael P. Erb, Tony E. Wong, Zhengyu Liu, and David Noone. 2018.  
1068 "Interpreting Precession-driven  $\delta^{18}\text{O}$  Variability in the South Asian Monsoon  
1069 Region." *Journal of Geophysical Research Atmospheres* 123 (11): 5927–46.
- 1070 Tharammal, Thejna, Govindasamy Bala, and David Noone. 2017. "Impact of Deep  
1071 Convection on the Isotopic Amount Effect in Tropical Precipitation." *Journal of  
1072 Geophysical Research Atmospheres* 122 (3): 1505–23.
- 1073 Tharammal, Thejna, Govindasamy Bala, and Jesse M. Nusbaumer. 2023. "Sources  
1074 of Water Vapor and Their Effects on Water Isotopes in Precipitation in the Indian  
1075 Monsoon Region: A Model-Based Assessment." *Scientific Reports* 13 (1): 708.
- 1076 Tharammal, Thejna, André Paul, Ute Merkel, and D. Noone. "Influence of Last  
1077 Glacial Maximum boundary conditions on the global water isotope distribution in  
1078 an atmospheric general circulation model." *Climate of the Past* 9, no. 2 (2013):  
1079 789-809.
- 1080 Tierney, Jessica E., Christopher J. Poulsen, Isabel P. Montañez, Tripti Bhattacharya,  
1081 Ran Feng, Heather L. Ford, Bärbel Hönlisch, et al. 2020a. "Past Climates Inform  
1082 Our Future." *Science* 370 (6517). <https://doi.org/10.1126/science.aay3701>.
- 1083 Tierney, Jessica E., Jiang Zhu, Jonathan King, Steven B. Malevich, Gregory J.  
1084 Hakim, and Christopher J. Poulsen. 2020b. "Glacial Cooling and Climate  
1085 Sensitivity Revisited." *Nature* 584 (7822): 569–73.
- 1086 Tiwari, Manish, Ashutosh K. Singh, and Rengaswamy Ramesh. 2011. "High-  
1087 Resolution Monsoon Records since Last Glacial Maximum: A Comparison of  
1088 Marine and Terrestrial Paleoarchives from South Asia." *Journal of Geological  
1089 Research* 2011 (August):1–12.
- 1090 Trenberth, K. E. 2011. "Changes in Precipitation with Climate Change." *Climate  
1091 Research* 47 (1): 123–38.
- 1092 Vidya, P.J., M. Ravichandran, M. P. Subeesh, Sourav Chatterjee, and Nuncio M.  
1093 2020. "Global Warming Hiatus Contributed Weakening of the Mascarene High in  
1094 the Southern Indian Ocean." *Scientific Reports* 10 (1): 3255.

Deleted: P J,

Field Code Changed

Field Code Changed

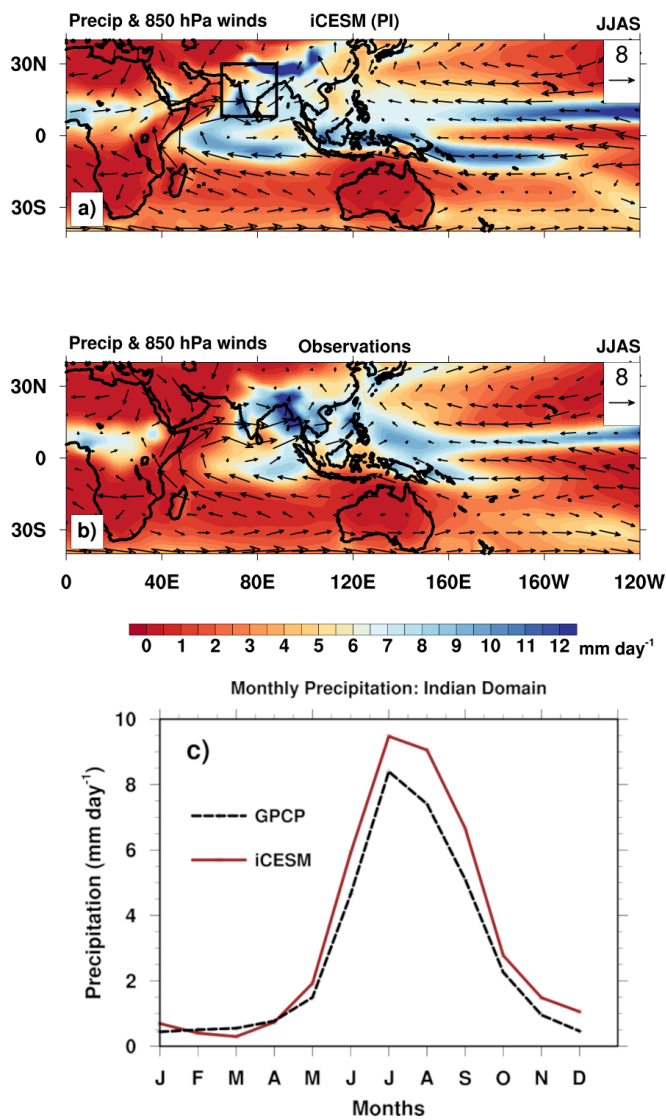
Field Code Changed

- 1097 Wang, Bin, M. Biasutti, M. Byrne, C. Castro, Chih-Pei Chang, K. Cook, R. Fu, et al.  
1098 2020. "Monsoons Climate Change Assessment." *Bulletin of the American*  
1099 *Meteorological Society* 102 (1): E1–19.
- 1100 Wang, Ting, Na Wang, and Dabang Jiang. 2023. "Last Glacial Maximum ITCZ  
1101 Changes from PMIP3/4 Simulations." *Journal of Geophysical Research*  
1102 *Atmospheres* 128 (10). <https://doi.org/10.1029/2022jd038103>.
- 1103 Webster, Peter J., and Song Yang. 1992. "Monsoon and ENSO: Selectively  
1104 Interactive Systems." *Quarterly Journal of the Royal Meteorological Society.*  
1105 *Royal Meteorological Society (Great Britain)* 118 (507): 877–926.
- 1106 Weldeab, Syee, Carsten Rühlemann, Qinghua Ding, Vyacheslav Khon, Birgit  
1107 Schneider, and William R. Gray. 2022. "Impact of Indian Ocean Surface  
1108 Temperature Gradient Reversals on the Indian Summer Monsoon." *Earth and*  
1109 *Planetary Science Letters* 578 (117327): 117327.
- 1110 Windler, Grace, Jessica E. Tierney, Jiang Zhu, and Christopher J. Poulsen. 2020.  
1111 "Unraveling Glacial Hydroclimate in the Indo-pacific Warm Pool: Perspectives  
1112 from Water Isotopes." *Paleoceanography and Paleoclimatology* 35 (12).  
1113 <https://doi.org/10.1029/2020pa003985>.
- 1114 [Worden, John, David Noone, and Kevin Bowman. 2007. "Importance of rain](#)  
1115 [evaporation and continental convection in the tropical water cycle." \*Nature\* 445,](#)  
1116 [no. 7127: 528-532.](#)
- 1117 Xavier, Prince K., Charline Marzin, and B. N. Goswami. 2007. "An Objective  
1118 Definition of the Indian Summer Monsoon Season and a New Perspective on  
1119 the ENSO–monsoon Relationship." *Quarterly Journal of the Royal*  
1120 *Meteorological Society. Royal Meteorological Society (Great Britain)* 133 (624):  
1121 749–64.
- 1122 Xue, Feng, Huijun Wang, and Jinhai He. 2003. "Interannual Variability of Mascarene  
1123 High and Australian High and Their Influences on Summer Rainfall over East  
1124 Asia." *Kexue Tongbao [Chinese Science Bulletin]* 48 (5): 492–97.
- 1125 Yadava, M. G., R. Ramesh, and G. B. Pant. 2004. "Past Monsoon Rainfall Variations  
1126 in Peninsular India Recorded in a 331-Year-Old Speleothem." *Holocene.*  
1127 <https://journals.sagepub.com/doi/pdf/10.1191/0959683604hl728rp>.
- 1128 Yanase, W., and A. Abe-Ouchi. 2007. "The LGM Surface Climate and Atmospheric  
1129 Circulation over East Asia and the North Pacific in the PMIP2 Coupled Model  
1130 Simulations." *Climate of the Past* 3 (3): 439–51.

- 1131 Yan, Mi, Bin Wang, and Jian Liu. 2016. "Global Monsoon Change during the Last  
1132 Glacial Maximum: A Multi-Model Study." *Climate Dynamics* 47 (1-2): 359–74.
- 1133 Zhu, Jiang, Zhengyu Liu, Esther Brady, Bette Otto-Bliesner, Jiaxu Zhang, David  
1134 Noone, Robert Tomas, et al. 2017. "Reduced ENSO Variability at the LGM  
1135 Revealed by an Isotope-enabled Earth System Model." *Geophysical Research*  
1136 *Letters* 44 (13): 6984–92.
- 1137 Zhu, Jiang, Bette L. Otto-Bliesner, Esther C. Brady, Andrew Gettelman, Julio T.  
1138 Bacmeister, Richard B. Neale, Christopher J. Poulsen, Jonah K. Shaw, Zachary  
1139 S. McGraw, and Jennifer E. Kay. 2022. "LGM Paleoclimate Constraints Inform  
1140 Cloud Parameterizations and Equilibrium Climate Sensitivity in CESM2." *Journal*  
1141 *of Advances in Modeling Earth Systems* 14 (4).  
1142 <https://doi.org/10.1029/2021ms002776>.
- 1143 Zhu, Jiang, and Christopher J. Poulsen. 2021. "Last Glacial Maximum (LGM) Climate  
1144 Forcing and Ocean Dynamical Feedback and Their Implications for Estimating  
1145 Climate Sensitivity." *Climate of the Past* 17 (1): 253–67.

1146  
1147  
1148  
1149  
1150  
1151  
1152  
1153  
1154  
1155  
1156  
1157

1158 **Main Figures**



1159  
 1160 Figure 1: Model-simulated and observed precipitation (shaded, mm day<sup>-1</sup>) and 850  
 1161 hPa winds (vectors in m s<sup>-1</sup>, reference vectors are shown in the panels) for the  
 1162 summer monsoon season (mean of June-July-August-September-JJAS). Panel (a)  
 1163 shows the simulated JJAS mean precipitation and 850 hPa winds from the iCESM  
 1164 Pre-Industrial (PI) simulation. Panel (b) shows the corresponding JJAS long-term  
 1165 mean precipitation from GPCP (Adler et al., 2018) and 850 hPa winds from ERA5  
 1166 reanalysis (1980-2000; Hersbach et al., 2020). Panel (c) shows the monthly mean

1167 precipitation averaged over the land grid cells in the Indian domain (8°N-30°N, 65°E-  
1168 88°E; black box in panel a, comparing the iCESM simulation with GPCP  
1169 observations.

1170

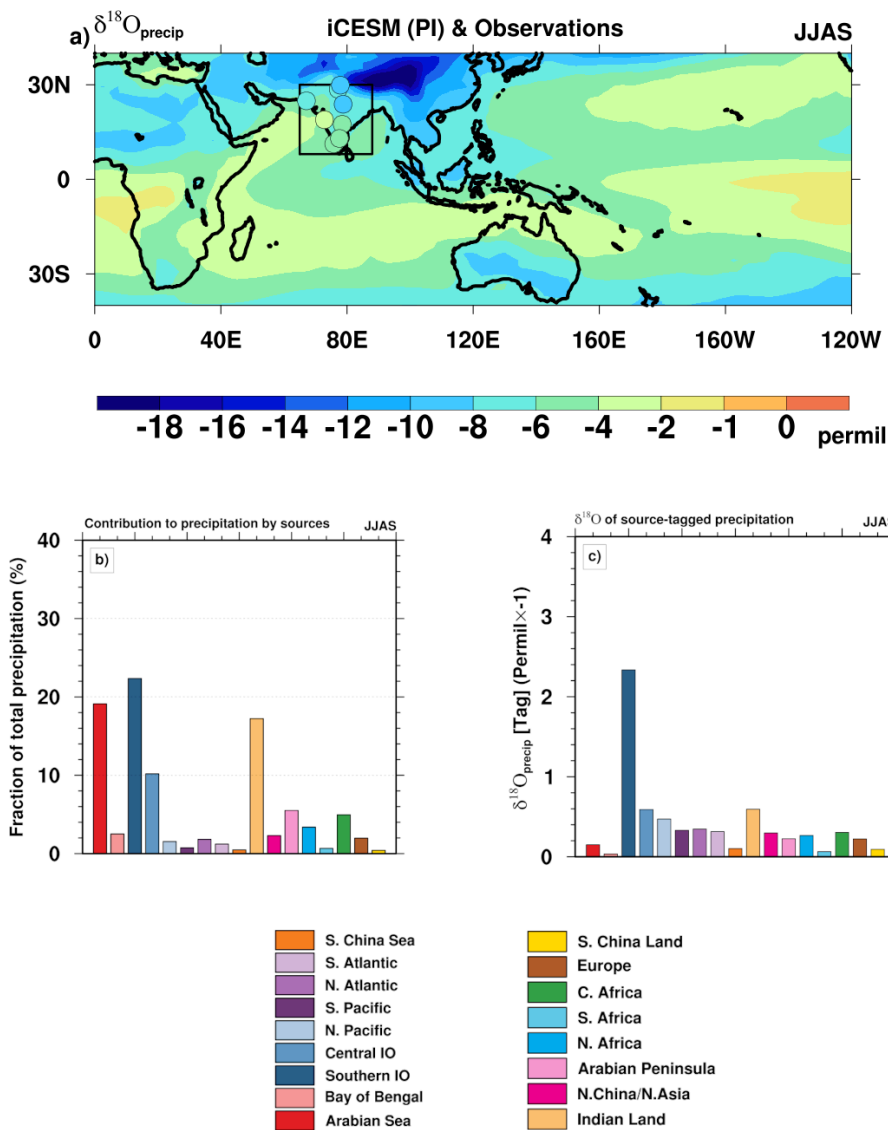
1171

1172

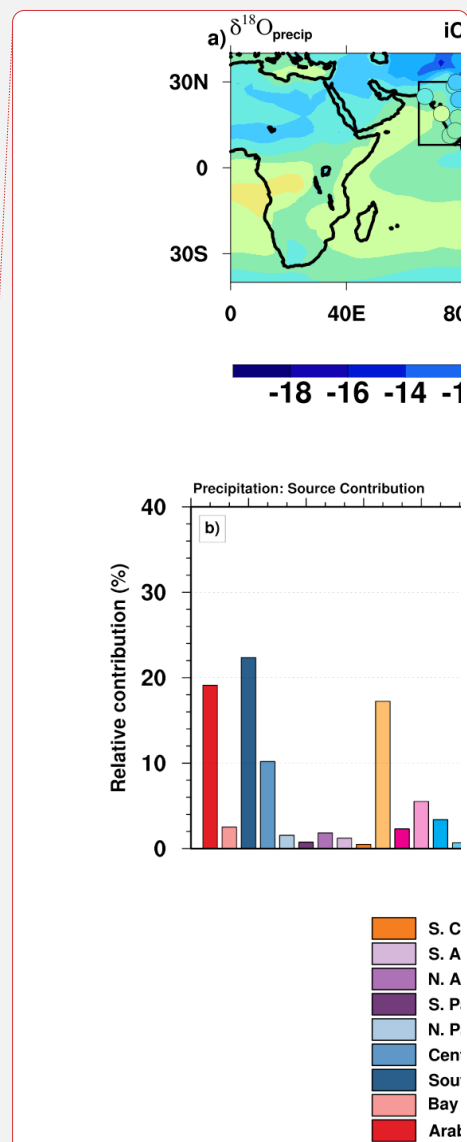
1173

1174

1175

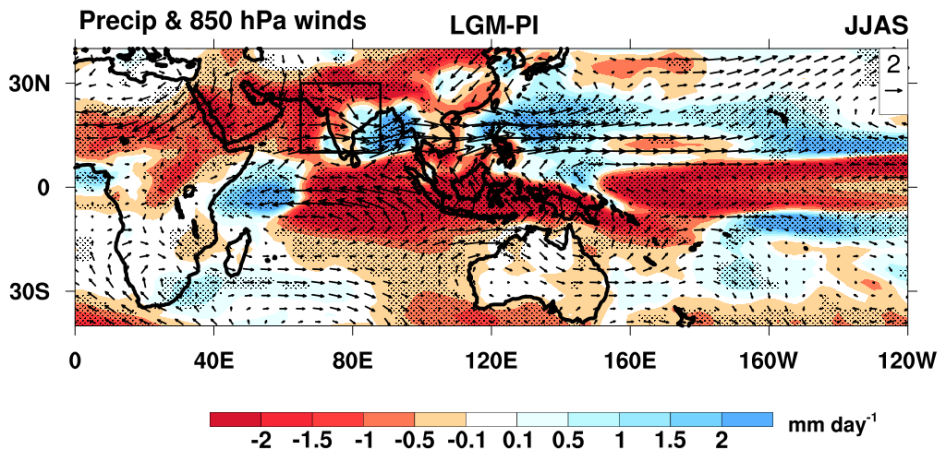


1176  
 1177 Figure 2: Isotopic composition of precipitation ( $\delta^{18}\text{O}_{\text{precip}}$ ) for the Indian summer  
 1178 monsoon season in the pre-industrial (PI) simulation, shown along with relative  
 1179 contribution of precipitation from the tagged sources, and their  $\delta^{18}\text{O}$  values in  
 1180 precipitation (weighted by relative contribution of precipitation).  
 1181 Panel (a) shows the mean JJAS  $\delta^{18}\text{O}_{\text{precip}}$  (shading, in permil [‰]). The filled circles  
 1182 in the Indian domain ( $8^{\circ}\text{N}$ - $30^{\circ}\text{N}$ ,  $65^{\circ}\text{E}$ - $88^{\circ}\text{E}$ ; shown in black box in panel a) represent



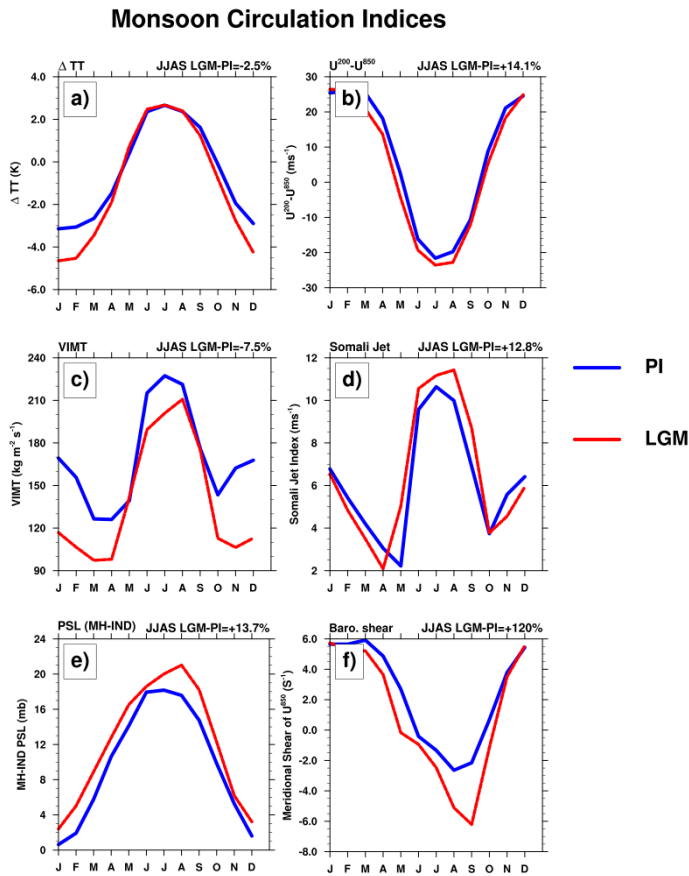
Deleted:

1184 long-term JJAS mean observational data from Global Network of Isotopes in  
1185 Precipitation (GNIP) stations. Panel (b) shows the relative contribution ( $P_{\text{tag}}/P_{\text{total}}$ , in  
1186 %) of precipitation to the Indian summer monsoon domain from 17 tagged water  
1187 vapor source regions. Panel (c) shows the  $\delta^{18}\text{O}_{\text{precip}}$  of tagged precipitation from the  
1188 17 different source regions that contribute to the Indian monsoon precipitation. The  
1189 y-axis values in panel (c) are multiplied by -1 for visualization purposes (units of ‰).  
1190  
1191  
1192  
1193  
1194  
1195  
1196  
1197  
1198  
1199  
1200  
1201  
1202  
1203  
1204  
1205  
1206  
1207  
1208  
1209  
1210  
1211  
1212



1213  
 1214  
 1215 Figure 3: The simulated differences in JJAS mean precipitation (shaded, in mm  
 1216 day<sup>-1</sup>) and low-level winds (850 hPa, vectors shown in m s<sup>-1</sup>) between the pre-  
 1217 industrial and the Last Glacial Maximum (LGM) simulations, shown as LGM-PI. The  
 1218 Indian domain is shown in black box. Regions where the anomalies are statistically  
 1219 significant at the 95% confidence level are stippled. Significance level is estimated  
 1220 using a Student's t test from a sample of 20 annual means from the control and LGM  
 1221 simulations.

1222  
 1223  
 1224  
 1225  
 1226  
 1227  
 1228  
 1229  
 1230  
 1231  
 1232  
 1233  
 1234  
 1235  
 1236  
 1237  
 1238



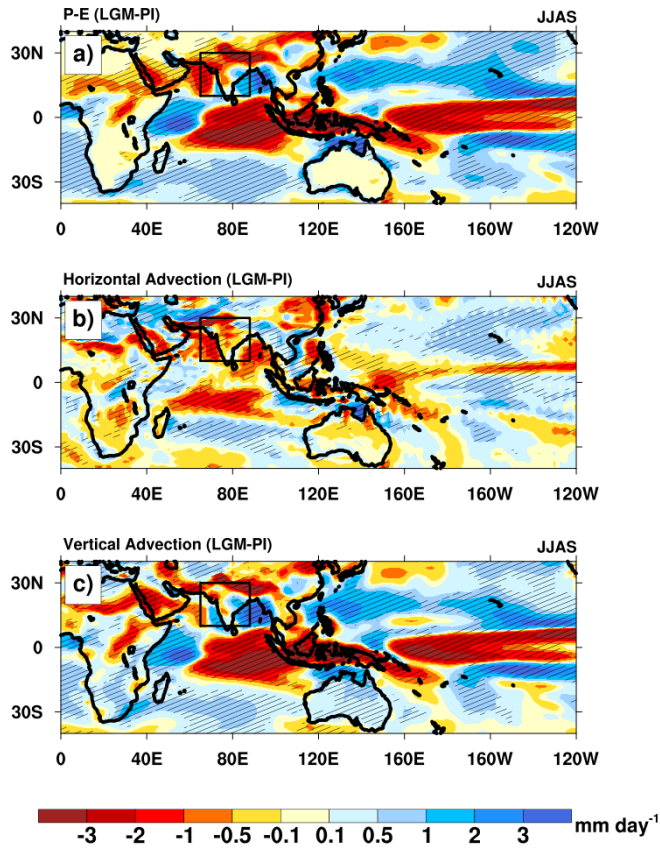
1240

1241 [Figure 4: Monsoon circulation indices calculated from the monthly means of PI and](#)  
 1242 [LGM simulations. The geographical areas for the calculations are shown in Figure](#)  
 1243 [S2b. JJAS mean values of differences between LGM and PI as \(LGM-PI\) in % is](#)  
 1244 [shown in the right top of each panel.](#)

1246 [Panel a\) shows the tropospheric temperature gradient \( \$\Delta TT\$ \) between the northern](#)  
 1247 [box \( \$10^{\circ}\text{N} - 35^{\circ}\text{N}\$ ,  \$30^{\circ}\text{E} - 110^{\circ}\text{E}\$ \) and the southern box \( \$15^{\circ}\text{S} - 10^{\circ}\text{N}\$ ,  \$30^{\circ}\text{E} - 110^{\circ}\text{E}\$ \).](#)  
 1248 [Panel b\) shows the vertical shear of zonal winds \( \$u\$  in  \$\text{m s}^{-1}\$ \) calculated as the change](#)  
 1249 [between  \$U^{850}\$  and  \$U^{200}\$  \( \$U^{850} - U^{200}\$ \) averaged over the region \( \$10^{\circ}\text{N} - 30^{\circ}\text{N}\$ ,  \$50^{\circ}\text{E} -\$](#)   
 1250  [\$95^{\circ}\text{E}\$ \).](#)  
 1251 [Panel c\) shows the hydrological index, calculated by averaging the Vertically](#)  
 1252 [Integrated Moisture Transport \(VIMT\) in the Indian Ocean-Arabian Sea region,](#)  
 1253 [\[ \$20^{\circ}\text{S} - 30^{\circ}\text{N}\$ ,  \$40^{\circ}\text{E} - 100^{\circ}\text{E}\$ \].](#)  
 1254 [Panel d\) shows Somali jet speed index, calculated as the square root of twice the area-averaged kinetic energy of 850 hPa horizontal winds over the region \( \$5^{\circ}\text{S} - 20^{\circ}\text{N}\$ ,  \$50^{\circ}\text{E} - 70^{\circ}\text{E}\$ \).](#)  
 1255 [Panel e\) shows the mean sea-level pressure](#)

Formatted: Superscript

1255 difference between the Mascarene high (MH; 20°S-40°S, 45°E-100°E) and the wider  
1256 Indian summer monsoon region (10°N-35°N, 45°E-100°E. Panel f) shows the  
1257 barotropic shear estimated over 10°N-26°N, 70°E-90°E.  
1258



1260

1261

1262

1263

1264

1265

1266

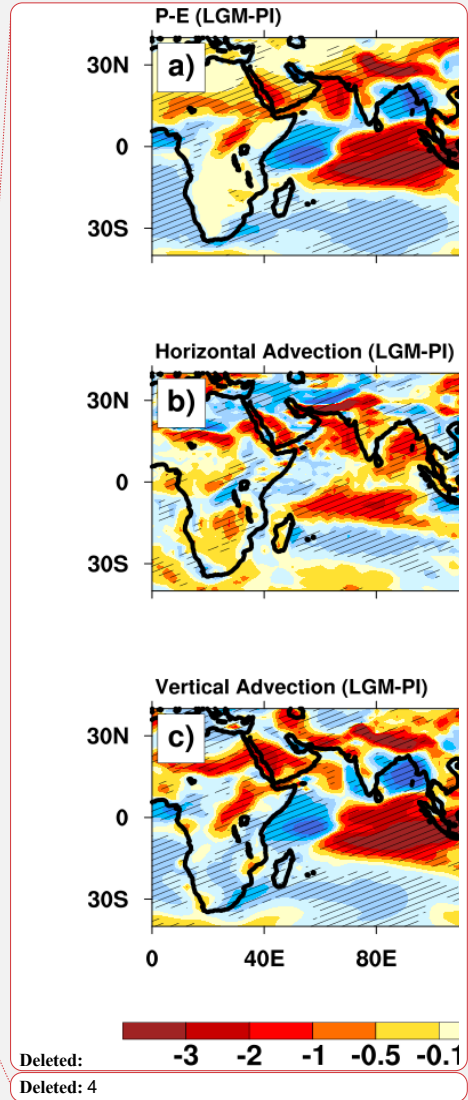
1267

1268

1269

1270

Figure 5: Changes in the JJAS mean atmospheric moisture budget between the LGM and the PI simulations, shown as LGM-PI. The panels show the components of the vertically integrated moisture budget anomaly: Panel a) shows anomalies in precipitation minus evaporation (P-E). Panel b) shows anomaly in horizontal water vapor advection ( $-\langle \mathbf{v} \cdot \nabla q \rangle$ ). Panel c) shows anomaly in vertical water vapor advection ( $-\langle \omega \partial q / \partial p \rangle$ ).  $\mathbf{v}$  is the horizontal wind,  $q$  specific humidity,  $p$  atmospheric pressure, and  $\omega$  pressure velocity. The Indian domain is shown in black boxes in the panels. All panels have the units of  $\text{mm day}^{-1}$ . The hatching shows regions where the anomalies are statistically significant at the 95% confidence level. Significance



1274 level is estimated using a Student's t test from a sample of 20 annual means from  
1275 the control and LGM simulations.

1276

1277

1278

1279

1280

1281

1282

1283

1284

1285

1286

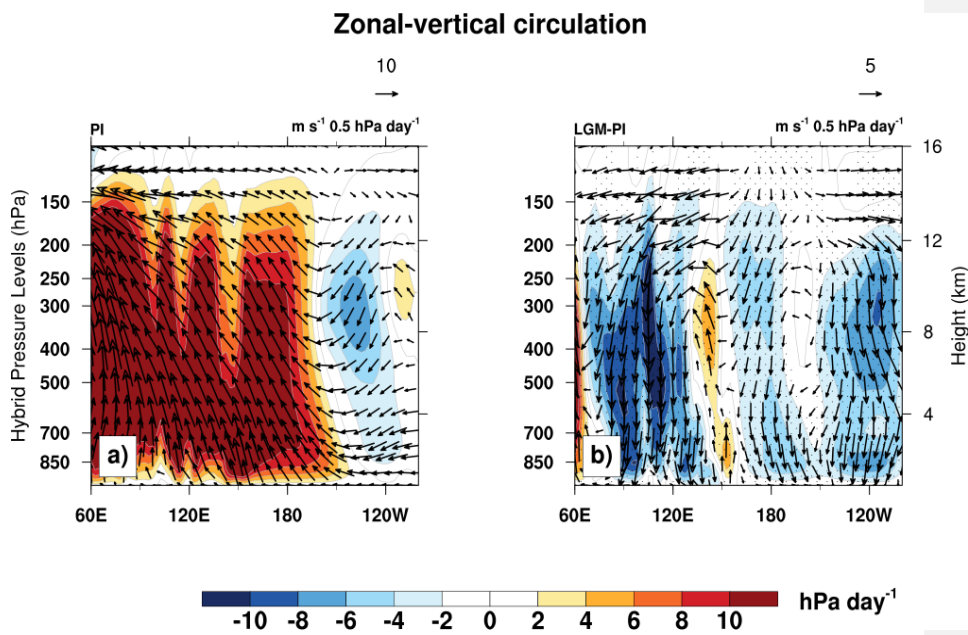
1287

1288

1289

1290

1291



1292

1293 Figure 6: The tropical zonal circulation during the JJAS season, averaged between  
 1294 10°S and 10°N. Panel a) shows the circulation in the PI control simulation, and the  
 1295 right panel b) shows the anomalies between the LGM and PI simulations (as LGM-  
 1296 PI). In both panels, shading represents the vertical pressure velocity ( $-\omega$ ), where blue  
 1297 shading indicates downward motion and red shading indicates upward motion. The  
 1298 vectors show the zonal-vertical circulation, composed of zonal wind ( $u$ , in  $\text{m s}^{-1}$ ) and  
 1299 vertical pressure velocity ( $-\omega$ ), with the  $\omega$  scaled by  $0.5 \text{ hPa day}^{-1}$  for visualization.  
 1300 The reference vectors are shown in the top right of the panels. The stippling in panel  
 1301 b) shows regions where the anomalies are statistically significant at the 95%  
 1302 confidence level. Significance level is estimated using a Student's t test from a  
 1303 sample of 20 annual means from the control and LGM simulations.

1304

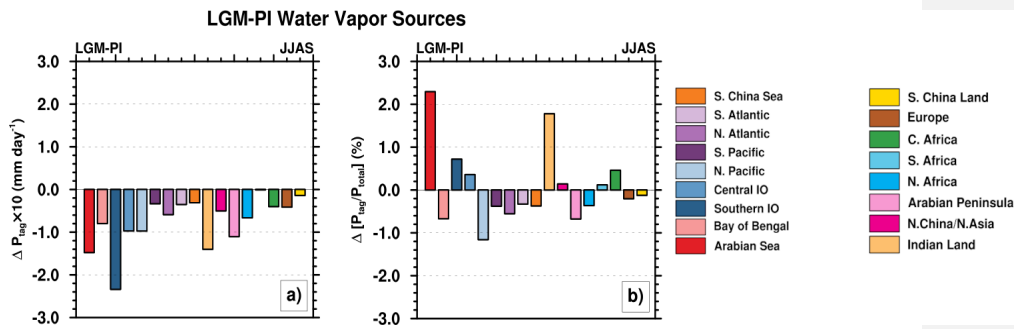
1305

1306

1307

Deleted: 5

1309  
1310  
1311



1312

1313 Figure 7: Changes in the precipitation contribution from 17 tagged moisture source  
1314 regions to the Indian monsoon domain's JJAS mean precipitation between the LGM  
1315 and the PI simulations. The source regions corresponding to each bar are identified  
1316 in the legend. Panel (a) shows the absolute difference in precipitation contribution  
1317 from each source region ( $\Delta P_{tag}$ ). The values are shown in mm day<sup>-1</sup> and have been  
1318 scaled up by a factor of 10 for visualization. Panel (b) shows the difference in the  
1319 relative contribution of each source to the total precipitation at the Indian monsoon  
1320 domain ( $\Delta [P_{tag}/P_{total}]$ ), shown as a percentage (%).

1321

1322

1323

1324

1325

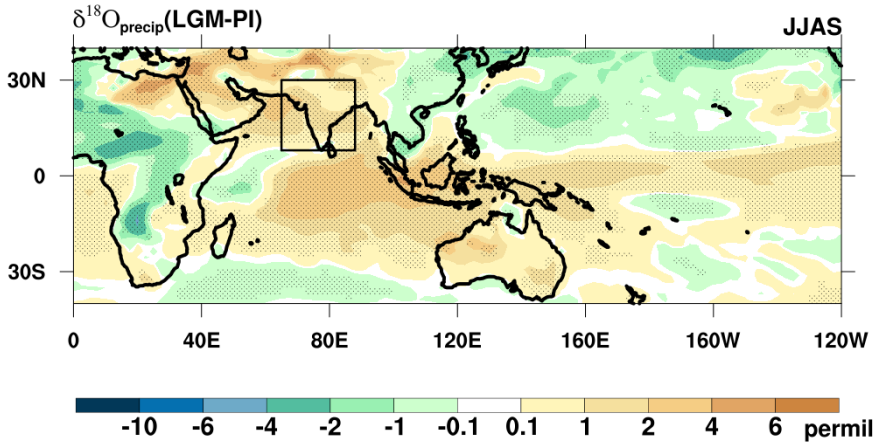
1326

1327

1328

Deleted: 6

1330



1331

1332 Figure 8: The anomalies of JJAS mean precipitation weighted  $\delta^{18}\text{O}_{\text{precip}}$  in permil  
1333 between the LGM and PI simulations as LGM-PI. The Indian monsoon domain is  
1334 shown in a black box in the plot. Regions where the anomalies are statistically  
1335 significant at the 95% confidence level are stippled. Significance level is estimated  
1336 using a Student's t test from a sample of 20 annual means from the PI control and  
1337 LGM simulations.

Deleted: 7

1338

1339

1340

1341

1342

1343

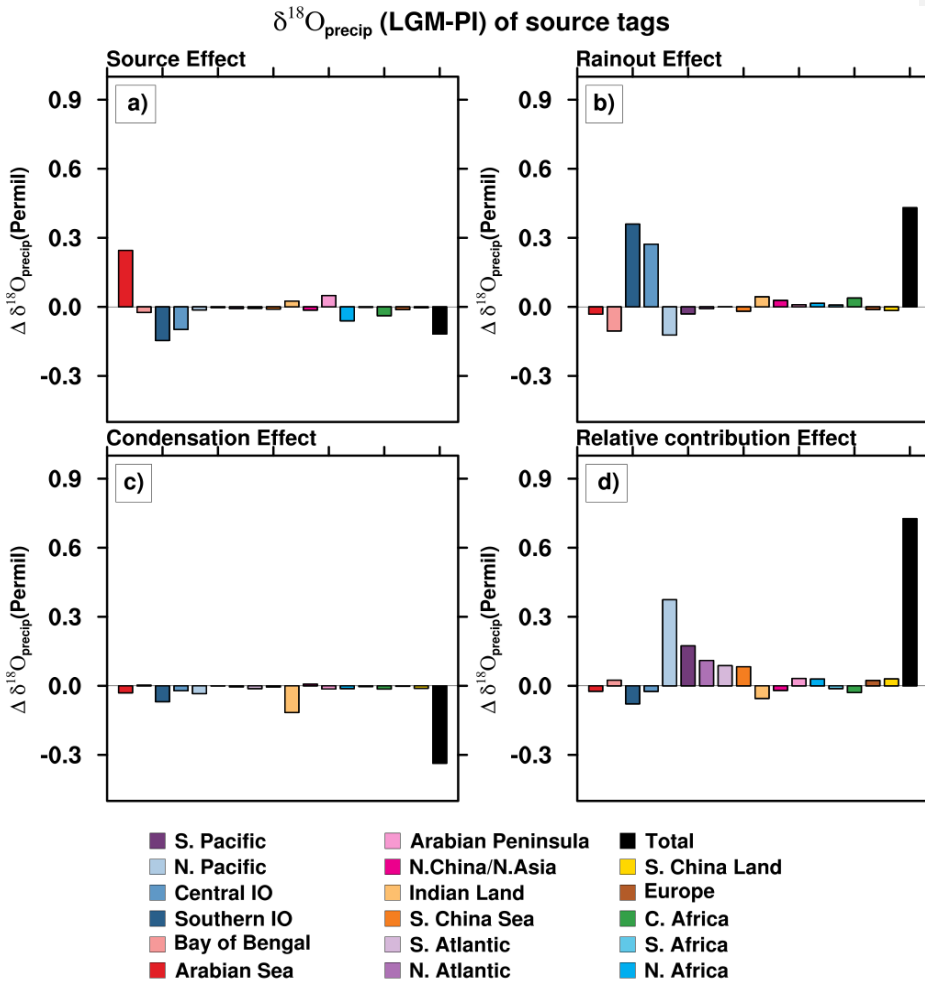
1344

1345

1346

1348

1349



1350

1351 Figure 9: Decomposition of the change in JJAS mean precipitation  $\delta^{18}\text{O}$  ( $\Delta\delta^{18}\text{O}_{\text{precip}}$ )  
 1352 for the Indian monsoon domain between the LGM and PI simulations. All values are  
 1353 in permil (‰). The  $\Delta\delta^{18}\text{O}_{\text{precip}}$  is divided into contributions from 17 tagged moisture  
 1354 source regions, shown in the legend. The decomposition separates the total anomaly  
 1355 into four primary physical processes for each tag. Panel a) shows the **Source Effect**:  
 1356 Changes in the  $\delta^{18}\text{O}$  of water vapor at its evaporative source. Panel b) shows the

Deleted: 8

Formatted: Font: Bold, Italic

1358 ***Rainout Effect***: Changes in isotopic composition due to rainout during atmospheric  
1359 transport from the source region to the ISM domain. Panel c) shows the  
1360 ***Condensation Effect***: Changes in the isotopic fractionation during the conversion of  
1361 water vapor to precipitation over the monsoon region. Panel d) shows the  
1362 ***Precipitation Relative Contribution Effect***: Changes in  $\delta^{18}\text{O}_{\text{precip}}$  for each tag  
1363 resulting from shifts in the relative contribution of precipitation from different source  
1364 regions.

Formatted: Font: Bold, Italic

Formatted: Font: Bold, Italic

Formatted: Font: Bold, Italic

1365

1366

1367

1368

1369